JGR Solid Earth

RESEARCH ARTICLE
10.1029/2018JB016242

Lithospheric Signature of Late Cenozoic Extension in Electrical Resistivity Structure of the Rio Grande Rift, New Mexico, USA

D. W. Feucht[1,2,3], **P. A. Bedrosian**[3], **and A. F. Sheehan**[1,2]

[1]Department of Geological Sciences, University of Colorado Boulder, Boulder, CO, USA, [2]Cooperative Institute for Research in Environmental Sciences, University of Colorado Boulder, Boulder, CO, USA, [3]Geology Geophysics and Geochemistry Science Center, U.S. Geological Survey, Denver, CO, USA

Key Points:
- We image 2-D anisotropic electric resistivity structure beneath the Rio Grande rift in New Mexico, USA, to depths of 200 km
- The lower crust beneath and laterally adjacent to the rift is exceptionally conductive along the entire rift axis
- The Rio Grande rift is electrically distinct from the Southern Basin and Range, the Colorado Plateau, and the Great Plains

Supporting Information:
- Supporting Information S1
- Data Set S1
- Data Set S2
- Data Set S3
- Data Set S4
- Data Set S5
- Data Set S6

Correspondence to:
D. W. Feucht,
daniel.feucht@colorado.edu

Citation:
Feucht, D. W., Bedrosian, P. A., & Sheehan, A. F. (2019). Lithospheric signature of late Cenozoic extension in electrical resistivity structure of the Rio Grande rift, New Mexico, USA. *Journal of Geophysical Research: Solid Earth*, *124*, 2331–2351. https://doi.org/10.1029/2018JB016242

Received 16 JUN 2018
Accepted 22 FEB 2019
Accepted article online 27 FEB 2019
Published online 28 MAR 2019

Abstract We present electrical resistivity models of the crust and upper mantle from two-dimensional (2-D) inversion of magnetotelluric (MT) data collected in the Rio Grande rift, New Mexico, USA. Previous geophysical studies of the lithosphere beneath the rift identified a low-velocity zone several hundred kilometers wide, suggesting that the upper mantle is characterized by a very broad zone of modified lithosphere. In contrast, the surface expression of the rift (e.g., high-angle normal faults and synrift sedimentary units) is confined to a narrow region a few tens of kilometers wide about the rift axis. MT data are uniquely suited to probing the depths of the lithosphere that fill the gap between surface geology and body wave seismic tomography, namely the middle to lower crust and uppermost mantle. We model the electrical resistivity structure of the lithosphere along two east-west trending profiles straddling the rift axis at the latitudes of 36.2 and 32.0°N. We present results from both isotropic and anisotropic 2-D inversions of MT data along these profiles, with a strong preference for the latter in our interpretation. A key feature of the anisotropic resistivity modeling is a broad (~200-km wide) zone of enhanced conductivity (<20 Ωm) in the middle to lower crust imaged beneath both profiles. We attribute this lower crustal conductor to the accumulation of free saline fluids and partial melt, a direct result of magmatic activity along the rift. High-conductivity anomalies in the midcrust and upper mantle are interpreted as fault zone alteration and partial melt, respectively.

1. Introduction

1.1. Tectonic Setting

The Rio Grande rift is a mid- to late-Cenozoic continental rift system in the southwestern United States that separates the Colorado Plateau and Basin and Range to the west from the stable North American interior to the east (e.g., Chapin & Cather, 1994; Keller et al., 1991; Tweto, 1979). The surface expression of the rift (Figures 1 and 2) consists of a series of elongate axial basins that form a north-south trending topographic depression through central Colorado and New Mexico before broadening into southern New Mexico and northern Mexico. The rift basins we observe today are, to first order, asymmetric half-grabens bounded on one side by a steeply dipping normal fault opposite a hinge zone. Prerift sedimentary units crop out on the rift flanks at elevations >3 km, and integrated geologic and geophysical modeling has imaged the base of rift fill at several kilometers below sea level in the Albuquerque basin, suggesting several kilometers of vertical offset on basin-bounding normal faults (Grauch & Connell, 2013). Synrift fill consists of Oligocene to Quaternary fluvial and lacustrine sedimentary units and volcanic rocks (Figure 1), with a prerift depositional surface of Paleocene-Oligocene units, Mesozoic or Paleozoic sedimentary units, and/or Proterozoic metamorphic rocks (Baldridge et al., 1983). The rift is named for the Rio Grande, a through-going river system that integrated the rift basins from the San Juan Mountains in Colorado to the Gulf of Mexico over the past 8 Myr (Repasch et al., 2017).

The earliest evidence of extension along the Rio Grande rift is Oligocene in age (e.g., Lipman & Mehnert, 1975). The extensional style of rifting varies both spatially along the rift axis from basin to basin, and temporally from rift initiation to the modern day (e.g., Chapin & Cather, 1994; Ricketts et al., 2015). Stratigraphic relationships observed in synrift sedimentary and volcanic units laid down in the Oligocene and early Miocene suggest that early rifting produced broad and shallow basins bounded by

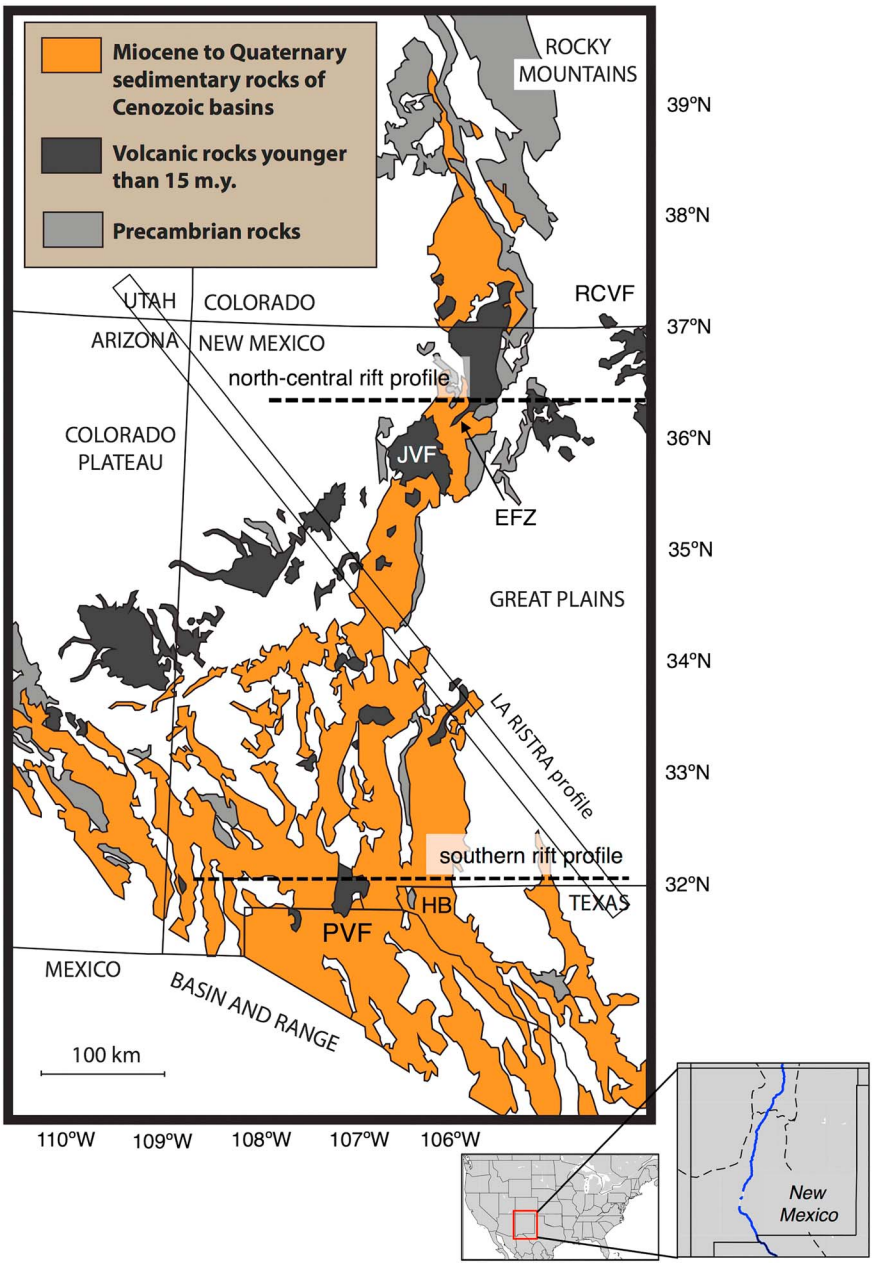

Figure 1. Simplified geologic map and tectonic setting of the Rio Grande rift (modified from Baldridge et al., 1983). Dashed lines are approximate locations of magnetotelluric profiles. Black rectangle indicates location of LA RISTRA seismic profile (Wilson et al., 2005). Relevant quaternary volcanic fields: Jemez volcanic field (JVF), Raton-Clayton volcanic field (RCVF), and Potrillo volcanic field (PVF). HB = Hueco Basin; EFZ = Embudo fault zone.

low-angle normal faults. As the rift evolved over time, there was a transition to a style of rifting that produced relatively narrow (typically less than 50-km wide), asymmetric rift grabens such as those we observe today. Estimates of crustal extension associated with the latter phase of rifting are modest, ranging from 8–12% in the San Luis Basin of south central Colorado (Kluth & Schaftenaar, 1994) to 28% in the southern Albuquerque basin of central New Mexico (Russell & Snelson, 1994). This north-to-south increase in extension, which is apparent in the footprint of mapped synrift sedimentary units (Figure 1), formed the basis for the hypothesis that the rift opened progressively from south to north. However, recent geochronologic studies on rift flank uplifts (Landman & Flowers, 2013; Ricketts et al., 2015) and petrologic studies of Miocene-Quaternary volcanic rocks in northern Colorado (e.g., Cosca

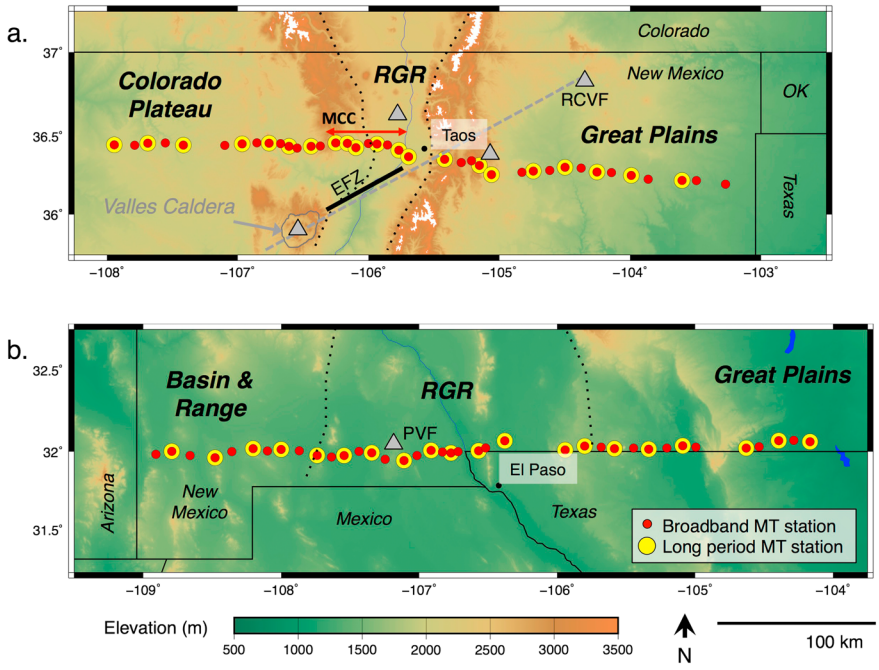

Figure 2. Map of magnetotelluric (MT) station locations for (a) north central rift and (b) southern rift profiles of the DRIFTER experiment. Yellow dots represent long-period MT recordings (3–6 weeks duration) and red dots are broadband MT recordings (18–48 duration). Black dotted lines show approximate physiographic boundaries of the Rio Grande rift (RGR). Topographic rim of Valles caldera in gray solid line, general trend of Jemez lineament in northern New Mexico shown by gray dashed line in (a). Solid black line is Embudo fault zone (EFZ; Bauer et al., 2016). Major late-Cenozoic volcanic centers labeled with gray triangles. Labeled volcanic centers as in Figure 1. Red arrow and MCC refers to lateral extent of midcrustal conductor in Figure 5c. OK = Oklahoma.

et al., 2014) demonstrate that this was not the case and that the rift opened simultaneously along its entire axis in the late Cenozoic. Modern geodetic observations reveal that the rift is actively extending at a rate of ~1 nanostrain/year (Berglund et al., 2012), with deformation over short timescales (~5 years) distributed regionally rather than focused on rift-bounding faults.

Volcanic activity associated with rifting is relatively minor compared to other continental rift systems of similar age and size (Keller et al., 1991). The most prominent volcanic feature in the region is the so-called Jemez lineament (Figure 2), a series of relatively young (~15 Ma to 3 ka) volcanic fields and lava flows that roughly follow a northeast trending line from southeast Arizona to northeast New Mexico (Aldrich, 1986). Although eruptive activity along the lineament is predominantly contemporaneous with the latter stage of rifting, the distribution of volcanic centers extends beyond the physiographic rift and the trend runs oblique to the central rift axis. Concentration of volcanic activity along the lineament may represent reactivation of a preexisting zone of weakness in the lithosphere that dates to the Proterozoic assembly of the North American continent (e.g., Magnani et al., 2004). In the central rift near Socorro, New Mexico, seismic reflection (Rinehart et al., 1979) and geodetic studies have identified a magmatic sill in the midcrust (~20-km depth), although there are no corresponding young volcanic rocks at the surface (NAVDAT database, Walker et al., 2006). Much of our understanding of the chemistry of the lower crust and upper mantle in the rift has come from petrologic work done on xenoliths from Kilbourne hole, a maar in the Potrillo volcanic field (Figure 1) created by a phreatomagmatic eruption 24 ka (Gile, 1987).

1.2. Previous Geophysical Results

1.2.1. Seismic Studies

The LA RISTRA seismic experiment (e.g., Gao et al., 2004; Gok et al., 2003; Wilson et al., 2005) was a high-resolution passive seismic study of crust and upper mantle structure beneath the Rio Grande rift. The array consisted of 54 broadband seismic stations deployed along a profile stretching 950 km diagonally across New

Mexico from the Four Corners region to west Texas (Figure 1). Gao et al. (2004) used *P* and *S* wave travel time residuals to image upper mantle velocity structure and found a broad, low-velocity zone several hundred kilometers wide centered on the rift and extending to depths >200 km. Imaging of high-velocity anomalies at greater depths beneath the rift margins led Gao et al. to interpret the rift-centered low-velocity zone as elevated temperatures within the upper mantle resulting from small-scale convection. Looking deeper, seismic receiver functions along the LA RISTRA profile (Wilson et al., 2005) revealed no significant deflection of the 410- or 660-km mantle transitions, suggesting that convection is confined to upper mantle flow rather than driven by a deep-sourced mantle plume. Examination of shear wave splitting directions (Gok et al., 2003) showed a consistent N40°E fast direction along the majority of the LA RISTRA profile. This result led the authors to conclude that the predominant driver of mantle seismic anisotropy beneath the rift is North American plate motion rather than active convection. Anomalous north-south oriented fast directions were detected beneath westernmost Texas, suggesting that east-west convection is more prominent in the southern rift (Gok et al., 2003).

At a broader scale, the EarthScope USArray seismic project has developed models of seismic velocity and velocity perturbations in the mantle for most of the United States, including the Rio Grande rift (e.g., Obrebski et al., 2011; Schmandt et al., 2015; Schmandt & Humphreys, 2010; Shen & Ritzwoller, 2016). All of these models indicate a region of relatively low velocity extending from the base of the crust into the upper mantle (>100-km depth) beneath the rift. Imaging techniques more sensitive to crustal structure (e.g., Fu & Li, 2015; Gilbert, 2012; Shen & Ritzwoller, 2016) further reveal a thinned crust beneath much of the Rio Grande rift in New Mexico. Near the latitude of Taos, New Mexico, the crust is thick beneath the Great Plains (~45 km) and the Colorado Plateau (~40 km) and thinner (~35 km) directly beneath the rift (Wilson et al., 2005). Farther south the crust is generally thinner across the entire state of New Mexico with minimum values beneath the rift of ~30 km (Fu & Li, 2015).

1.2.2. Electrical Resistivity Studies

The earliest investigations into the large-scale electrical resistivity structure of the Rio Grande rift were conducted by Hermance and Pedersen (1980). Using four long-period (>1,000 s) magnetotelluric (MT) soundings collected in two locations, Hermance and Pedersen identified a thin zone of high electrical conductance (conductivity thickness product of 1,600–2,200 Siemens) at midcrustal levels in both the north central rift near Santa Fe, New Mexico, and in the southern rift near El Paso, Texas. They associated the conductor with the then recently identified Socorro magma body (Rinehart et al., 1979) and concluded that a thin (~1-km thick) sill of basaltic magma could explain both the seismic results in Socorro and the MT results to the north and south. They proposed that the interpreted basaltic sill at midcrustal levels was a ubiquitous feature of the Rio Grande rift given that they observed similar conductive features several hundred kilometers apart along the rift axis.

Subsequent MT investigations near the Socorro magma body by Jiracek et al. (1983) introduced a competing interpretation for high crustal conductivity in the Rio Grande rift: saline fluids. Jiracek et al. did not image a midcrustal conductor beneath Socorro, prompting them to reinterpret the results of Hermance and Pedersen (1980). The new hypothesis was that recent magmatic injection into the upper crust at Socorro had breached an impermeable layer in the midcrust that had previously trapped a high volume of saline fluid (i.e., the conductor imaged beneath Santa Fe and El Paso). Networks of free saline aqueous fluid, often interpreted to be interconnected along grain boundaries in addition to fracture networks, have been proposed to explain midcrustal conductors in other active tectonic environments (e.g., the Basin and Range, Wannamaker et al., 2008, and Tibet, Li et al., 2003). Although geomagnetic depth soundings (i.e., three-component measurements of the naturally occurring time varying magnetic field) collected at Socorro by Hermance and Neumann (1991) later confirmed the existence of a high-conductivity layer in the lower crust, the identity of the conductivity mechanism responsible for the anomaly is still an open question.

Numerous other electrical resistivity studies conducted in the Rio Grande rift have focused on smaller and/or shallower geophysical targets rather than deep or lithosphere-scale features. The resistivity structure of the Jemez Mountains volcanic complex, the largest volcanic center along the Jemez lineament and source of two massive caldera-forming eruptions in the Holocene, has been investigated for geothermal potential (e.g., Hermance, 1979) and tectonic interpretation (Jiracek et al., 1996; Nettleton, 1997). Those studies reveal an electrically conductive body beneath the Valles caldera that coincides with an imaged

low-velocity zone (e.g., Steck et al., 1998), the top of which lies at 5–15 km beneath the surface. Unfortunately, a narrow station distribution and the lack of 3-D MT modeling capabilities at the time prevented further characterization of the geometry of the conductor, hindering its interpretation in a regional tectonic context.

The U.S. Geological Survey has conducted numerous MT studies of the rift basins in southern Colorado and northern New Mexico (e.g., Rodriguez & Sawyer, 2013). Those studies have generally focused on interpreting stratigraphic relationships and shallow geologic structure rather than large-scale tectonic features.

The Summer of Applied Geophysical Experience field course (Baldridge et al., 2012) has collected dozens of MT soundings in the Rio Grande rift in northern New Mexico. These MT data have been studied along with gravity and seismic data to image and interpret basin-scale structure of the Española Basin (Biehler et al., 1991). While these data are of sufficiently high quality and long period (>1,000 s) to image the midcrustal conductor first identified by Hermance and Pedersen (1980) near Santa Fe, New Mexico, the limited station distribution (all stations are within ~50 km of Santa Fe) prevents further characterization of this conductor's geometry beyond observations of its depth.

In this paper, we present modeling results from the first MT investigation of the Rio Grande rift that was expressly designed to image the lithospheric-scale electrical resistivity structure of the rift and the surrounding environment. This was achieved by a combination of (1) long-period MT instrumentation to sense structure at upper mantle depths, (2) wide-aperture profiles with dense station spacing and wide-band instrumentation to capture detailed crustal structure, and (3) purposeful collection of data off axis from the rift (e.g., over the Colorado Plateau and Great Plains) in order to discriminate rift-related structure from the tectonic collage on which it is superimposed.

2. Methods and Data

2.1. Magnetotellurics

The MT method is in particular sensitive to electrical resistivity, or its reciprocal conductivity, which is dependent upon mineralogy, fluid content, partial melt, and to lesser extents, pressure, and temperature. Sources of high conductivity in sedimentary basins and within the brittle upper crust include clay minerals, saturated zones with high permeability and porosity, and saline brines with high total dissolved solid content. The primary controls on electrical conductivity in the lower crust are the abundance and interconnectedness of aqueous fluid, small volumes of partial melt, and conductive mineralization, in particular graphite and sulfides. Electrical conductivity in the upper mantle is primarily controlled by the concentration of water in nominally anhydrous minerals (Dai & Karato, 2009; Poe et al., 2010), the presence of partial melt, and to a lesser extent the bulk temperature of the rock (Constable et al., 1992).

MT data are collected by measuring spatial and temporal variations in the naturally occurring electric (E) and magnetic (H) fields at the surface of the Earth. The MT impedance tensor (Z) is a second-rank complex tensor that in the frequency domain (with $\exp(+i\omega t)$ time dependence here) relates horizontal magnetic fields to horizontal electric fields by

$$\begin{bmatrix} E_X \\ E_Y \end{bmatrix} = \begin{bmatrix} Z_{XX} & Z_{XY} \\ Z_{YX} & Z_{YY} \end{bmatrix} \cdot \begin{bmatrix} H_X \\ H_Y \end{bmatrix} \tag{1}$$

When interpreting data in a strictly two-dimensional scenario, the x component of these horizontal electric and magnetic fields is aligned parallel to geoelectric strike of subsurface structures while the y component is aligned perpendicular to strike. Absent a priori knowledge of geoelectric strike, for example, during data acquisition, north and east are used as the positive x and y directions, respectively. This convention yields a z coordinate that is positive downward into the Earth in a right-hand coordinate system. In the case that geoelectric strike is discovered to differ from that assumed during acquisition, the impedance tensor may be rotated during data processing into any desired coordinate frame. MT data in this study are presented in the default coordinate system (north = x positive), as the assumed geoelectric strike of the Rio Grande rift is approximately north-south, parallel to the rift axis. The four components of the complex, frequency-

dependent impedance tensor (Z) can be represented as scaled amplitude (apparent resistivity, ρ_a, units of Ωm) and phase. The magnetic field transfer function (T), or tipper, is a complex unitless vector quantity that relates the horizontal magnetic-field to the vertical magnetic-field by

$$H_Z = [T_X \;\; T_Y] \cdot \begin{bmatrix} H_X \\ H_Y \end{bmatrix} \tag{2}$$

These transfer functions vary from station to station as the electrical resistivity structure of the subsurface varies and with frequency as a function of changes in subsurface resistivity with depth or distance from a single station. A MT sounding consists of estimates of impedance and tipper as a function of period, obtained via spectral analysis of electric field and magnetic field time series. The depth of investigation of each sounding depends on both the period (the inverse of frequency) and the local electrical resistivity structure, with longer periods and a more resistive subsurface permitting a greater depth of investigation.

2.2. DRIFTER MT Data

Seventy-three MT soundings were collected as part of the Deep Rift Electrical Resistivity (DRIFTER) experiment conducted in 2012 and 2013 (data available in U.S. Geological Survey data release (Feucht et al., 2018) hosted on ScienceBase https://doi.org/10.5066/F7610XTR). Data were collected along two 450-km-long profiles located at 36.2 and 32°N latitude (Figure 2). Five time series, consisting of two orthogonal components of the horizontal electric field and three orthogonal components of the magnetic-field, were recorded at each MT site. Broadband MT data (100 Hz-1,000 s) were collected on Electromagnetic Instruments low-frequency MT24 data loggers while long-period data (1–11,000 s) were collected on Narod Intelligent Magnetotelluric System (NIMS) data loggers. Three component magnetic field observations were made using orthogonal induction coils and fluxgate magnetometers, for broadband and long-period data, respectively. Electric field measurements were made using two orthogonal electric dipoles each consisting of two nonpolarizing electrodes connected by approximately 100 m of insulated copper wire. Each station was outfitted with broadband instrumentation for one to three nights and/or long-period instrumentation for up to 6 weeks (see Figure 2). Nominal station spacing was 5–15 km, with a select few data gaps of up to 30 km due to permitting and land access restrictions. Data were collected at several (2–8) stations simultaneously to permit remote-reference processing (Gamble et al., 1979). Time series processing and transfer function estimation were performed using the multistation remote reference processing of Egbert (1997). In general, the remote referenced data are of high quality, sufficient for producing robust transfer function estimates between 10 Hz and 3.000 s for most stations. Select stations with long period data have clean transfer function estimates to 10,000 s. Plots of representative data quality can be found in Figure S1 of the supporting information. Additionally, plots of apparent resistivity, phase, and tipper for every station used in this study may be found in the ScienceBase data release (Feucht et al., 2018).

2.3. Dimensionality

The MT method is sensitive to three-dimensional (3-D) Earth structure at a variety of scales. Near-surface heterogeneities in resistive structure that are of sufficiently small length-scale compared to the station spacing are considered sources of distortion (e.g., Groom & Bailey, 1989). Sufficiently large 3-D structure is of geologic interest and demands 3-D modeling. In this study we perform 2-D modeling of data collected along east to west oriented profiles. Justification of this approach requires validation of two assumptions. The first assumption is that the data are predominantly sensitive to a regional scale 2-D resistivity structure. In other words, 3-D features beneath or adjacent to our profile must either be sufficiently small in scale to be considered sources of distortion or sufficiently distant from our profile so as to not influence our MT observations. The second assumption is that there exists a single predominant 2-D trend, or geoelectric strike direction, to the regional resistivity structure that is oriented within at most a few tens of degrees of the direction orthogonal to the profile trace. We confirm that these two assumptions are valid for our data by examining the MT phase tensor and the magnetic transfer function, or tipper.

The magnetic field transfer function (T), or tipper, is a complex, unitless, frequency-dependent vector quantity that relates the horizontal components of the magnetic field to the vertical magnetic field. Tipper is often represented in map view as an induction vector, an arrow that points toward conductive anomalies. In the case of 2-D Earth structure, induction vectors point perpendicular to geoelectric strike. The quantity tipper

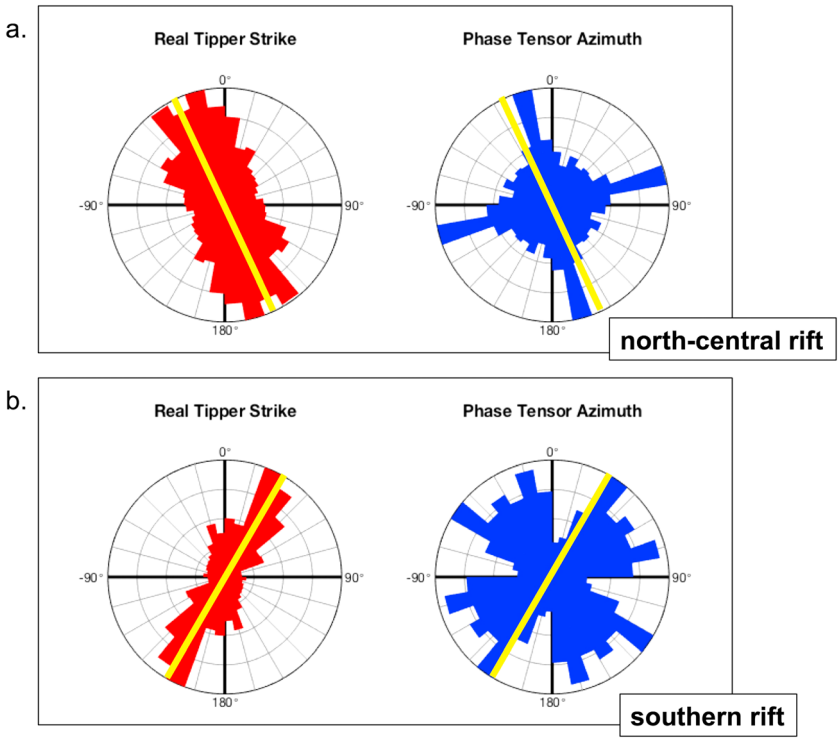

Figure 3. Dimensionality parameter rose diagrams for (a) north central rift and (b) southern rift MT stations. Tipper strike direction (left, red fill) and phase tensor principal axes orientations (right, blue fill) are shown. Both parameters have been filtered by period (T = 30–10,000 s) and phase tensor ellipticity (ϕ_{min}/ϕ_{max}). The latter criterion eliminates contamination from data at stations and frequencies for which phase tensor analysis indicates high noise ($\phi_{min}/\phi_{max} < 0.2$) or one-dimensional data ($\phi_{min}/\phi_{max} > 0.8$). The apparent 90° ambiguity in strike direction provided by phase tensor parameters is resolved by comparison to tipper strike direction. Predominant tipper strike directions (solid yellow lines) for both profiles appear to be within ±30° of the north-south trend of the rift axis. All data were rotated N25°W and N30°E, for north central rift and southern rift profiles, respectively, prior to 2-D inversion.

strike provides an indication of geoelectric strike (Figure 3) and is calculated by adding 90° to the azimuth of an induction vector.

The MT phase tensor (Caldwell et al., 2004) is a mathematical transformation of the impedance tensor that is represented in map view as an ellipse. The major and minor axes of the phase tensor ellipse are proportional to the rotationally invariant maximum and minimum principal values of the represented phase tensor, with noncircular ellipses indicating higher-order electrical resistivity structure (i.e., lateral variations in resistivity). In the 2-D case, the major axis of the ellipse will align either perpendicular or parallel to the predominant strike direction of a geoelectrical contact.

Figure 3 shows distributions of the real component of tipper strike and the orientation of the major and minor axes of phase tensor ellipses for both profiles at periods >30 s. Independent examination of phase tensor azimuth results in a 90° ambiguity in strike direction because the major axis of the phase tensor ellipse may be perpendicular or parallel to strike direction, depending on the local resistivity structure. This ambiguity is resolved by comparison to plots of tipper strike. Figure 3 reveals predominant strike directions for the north central rift and southern rift of N25 W and N30°E, respectively. The existence of a predominant tipper strike direction that (1) is consistent within each profile, (2) does not significantly vary with frequency, and (3) is supported by cross examination of phase tensor azimuth, provides justification for the 2-D inversion approach described below. To ensure proper modeling in the 2-D regime, MT data along each profile, including tipper, were rotated prior to inversion to match the corresponding strike direction.

There is a risk in MT modeling, especially in 2-D, that low-resistivity surface features such as sedimentary basins may bias the inversion results and introduce deep conductors into the model that do not accurately reflect the true resistivity structure (Folsom et al., 2017). For both profiles, the observed strike direction is

inconsistent with the trend of major surface features. The strike direction for the north central rift is almost orthogonal to regional geologic structures, including the Jemez lineament and the Embudo fault zone (EFZ; Bauer et al., 2016; Figure 2), both of which exhibit a NE-SW trend. In the southern rift, the major structural features of the upper crust include Laramide-age sedimentary basins that trend NW-SE (Averill & Miller, 2013) and axial basins of the Rio Grande rift that trend N-S. That the strike direction derived from MT dimensionality analysis does not match the structural grain of these major surface features suggests that the MT data are sensitive to deeper features within the crust and upper mantle and are not overly biased by the high-conductivity sedimentary basins of the Rio Grande rift.

Small-scale heterogeneity in the near-surface resistivity structure adjacent to an MT station may introduce a static shift, or galvanic distortion, into the apparent resistivity data at that site. We identified a total of six stations over both profiles that were likely subject to this type of distortion. We were able to mitigate the shift at these sites prior to inversion by employing the nearest-neighbor method, that is, comparing the apparent resistivity curves of multiple nearby stations to determine which of the modes was shifted and by how much.

2.4. The 2-D Magnetotelluric Inversion

Both isotropic and anisotropic inversion results were obtained using MARE2DEM (Key, 2016), which utilizes an Occam's inversion approach (DeGroot-Hedlin & Constable, 1990) to iteratively solve for the smoothest resistivity structure that adheres to a user-defined target data residual. MARE2DEM is a 2-D finite element regularized inversion developed for marine MT and controlled-source electromagnetic inversion problems but with functionality for terrestrial MT data as well. Prior to 2-D inversion, a minimum error threshold, or error floor, of 10% of the log amplitude of the apparent resistivity, and 2.8° in phase, was applied to the data. An error floor of 0.03 was applied to all tipper components used in the inversion (real and imaginary components of T_Y). Data errors exceeding the error floor were retained where available. The Supporting Information S1 contains additional details on the inversion algorithm, data selection, and mesh preparation, including starting model optimization.

Anisotropy for the purposes of this study refers to strictly horizontal (or transverse) anisotropy, wherein the electrical resistivity of each grid cell is allowed to vary in two directions: parallel (ρ_{yy}) and perpendicular (ρ_{xx}) to the profile trace. Because both of our profile traces are oriented nominally east-west, the ρ_{xx} models in this study show the resistivity structure that is sensed by electric fields flowing north-south, along the strike of the rift axis, while the ρ_{yy} model is the resistivity structure sensed by electric fields flowing east-west, across the rift. The degree of anisotropy for a particular region of the model can be visually approximated by the difference in grid cell resistivity between the two models. For example, $\rho_{xx} < \rho_{yy}$ indicates that horizontal electric currents will more readily flow north-south than east-west through that particular grid cell (i.e., the conductive geologic feature in that region of the model is oriented rift parallel). Where the resistivity values of the ρ_{xx} and ρ_{yy} models agree it may be assumed that anisotropic resistivity structure is not required to fit the data. Anisotropy is incorporated into the inversion through the model roughness term, which contains a measure of the difference between the ρ_{xx} and ρ_{yy} models, regularized by an anisotropy penalty factor, α. The value of α varies from 0 (completely anisotropic) to 1 (exclusively isotropic) and is defined by the user prior to inversion. For the anisotropic inverse models shown in this study we set $\alpha = 0.1$.

3. Results

3.1. Inversion Results

Figure 4 shows 2-D isotropic electrical resistivity models obtained by inverting the MT data along our two profiles. The isotropic models for both the north central rift (Figure 4a) and the southern rift (Figure 4b) achieved the target root-mean-square (RMS) value of 1.5 given the applied errors. This represents a reduction in data residual (nRMS) of ~86% relative to the best fitting half-space starting models of 80 and 30 Ωm (initial nRMS values of 8.31 and 8.55), for the north central and southern rift respectively. For comparison, anisotropic models of each profile (presented later, Figures 5 and 6) were able to achieve a slightly lower target RMS of 1.2. Attempts to drive the isotropic models to an RMS value of 1.2 resulted in exceedingly complex models and distinct overfitting (i.e., RMS < 1) of many data components. See the supporting information (Figures S2 and S3) for pseudo section plots of data fit as well as nRMS values for each data

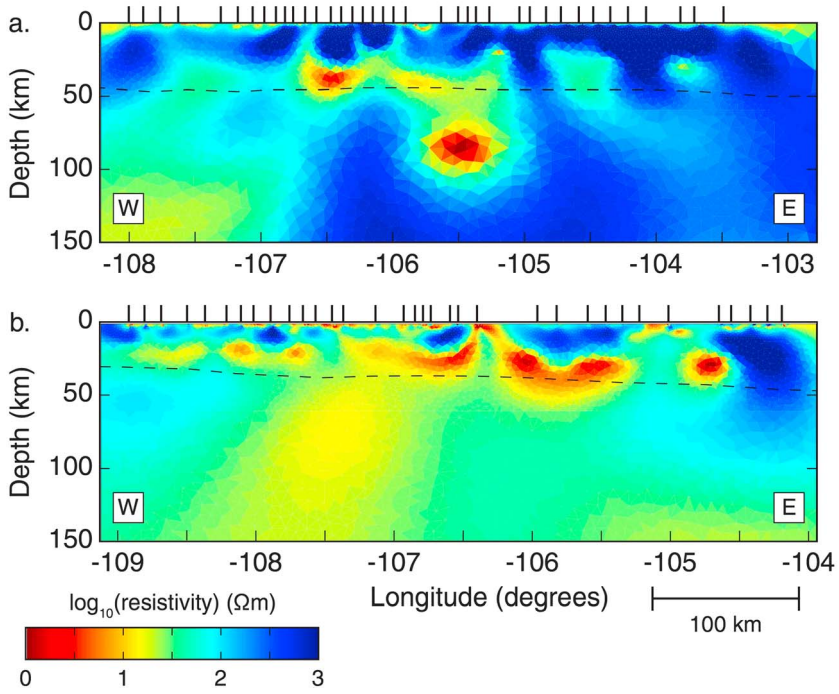

Figure 4. Isotropic resistivity models for (a) the north central rift and (b) the southern rift. The dashed line is an estimate of the crust-mantle boundary from joint inversion of receiver functions and phase velocity (Shen et al., 2013). Both models achieved a chi-square misfit of 1.5 and 2–3 iterations of model smoothing. Note the alternating vertical resistor-conductor-resistor pattern in the lower crust, particularly along the north central rift profile. This pattern is reminiscent of that generated from inverting anisotropic magnetotelluric data using a 2-D isotropic inversion routine (Heise & Pous, 2001).

component. In general, the best data fits were achieved for both real and imaginary components of inline tipper (T_Y) while Z_{xy} phase was often the most difficult to fit. The minimal enhancement in overall data fit achieved by the anisotropic inversion (from RMS 1.5 to 1.2), was not the only factor guiding our preference for the anisotropic models, as we outline below.

Present in both isotropic models is a distinct vertical resistor-conductor-resistor pattern in the middle and lower crust with a nominal wavelength of 25–50 km. There is no expectation from the surface geology or previous geophysical results to expect heterogeneity in the lower crust of this scale. This particular pattern in modeled resistivity structure closely resembles the results obtained by Heise and Pous (2001) in their investigation into the consequences of modeling anisotropic MT data using a 2-D isotropic inversion approach. For their study, Heise and Pous constructed synthetic resistivity models wherein one layer of an otherwise isotropic layer cake resistivity structure was assigned some degree of anisotropy. They then inverted the synthetic MT forward response to that model using a 2-D isotropic inversion code. The resulting resistivity model fit the data but modeled the anisotropic layer as a laterally alternating series of conductors and resistors, similar to the model features observed in the mid- to lower crust in Figures 4a and 4b. This was the first indication that modeling the resistivity structure of the lower crust beneath the Rio Grande rift may be improved by incorporating electrical anisotropy.

We concede that the distinct conductor-resistor-conductor pattern could be an artifact of 2-D inversion of 3-D isotropic structure. For example, conductive features that are off the profile and finite in length may project onto the profile as short wavelength anomalies. However, consistent phase splits and small tipper values (<0.2) observed for most stations (see supporting information) suggest that we are imaging a laterally coherent conductor rather than a series of finite conductive blobs distributed laterally across the lower crust or off profile.

Examination of pseudo-section plots of both isotropic and anisotropic modeling responses (see supporting information) reveals that either inversion approach produces a similar qualitatively acceptable fit to the data, given different target RMS values. However, to achieve a similar nRMS data misfit, the isotropic

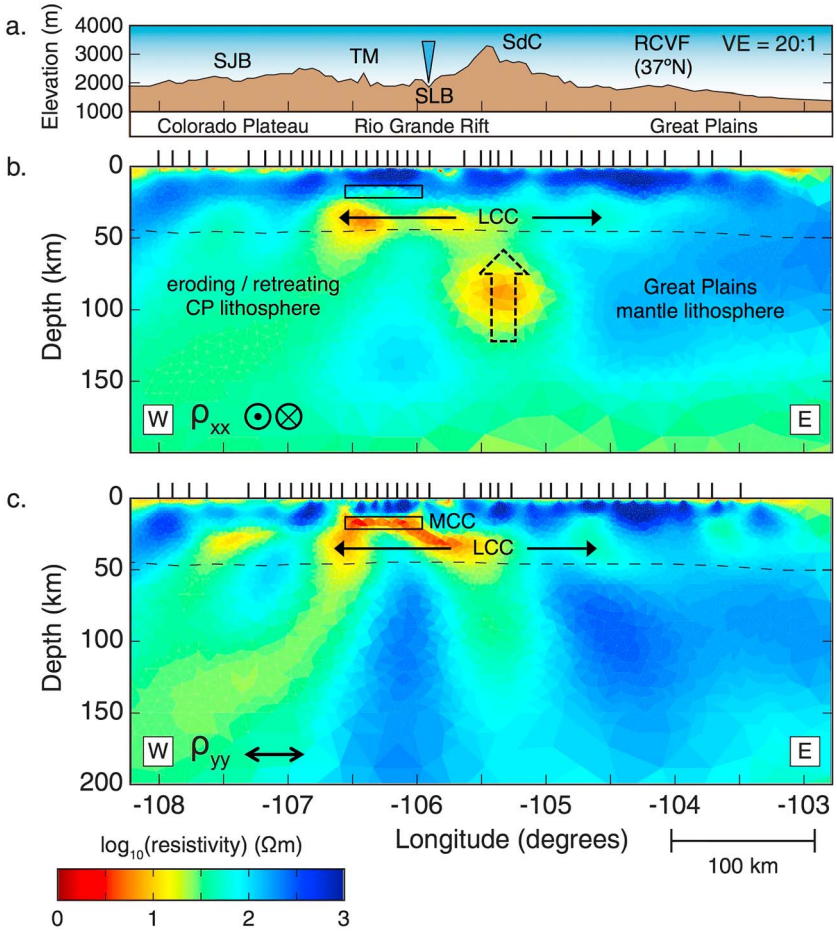

Figure 5. Anisotropic electrical resistivity model for north central rift (36.25°N). Includes a topography, (b) ρ_{xx} model, electrical resistivity structure sensed by north-south electric fields (parallel to the rift axis), and (c) ρ_{yy} model, electrical resistivity structure sensed by east-west electric fields (perpendicular to rift axis). Vertical tick marks at the surface indicate MT station locations. Inverted blue triangle indicates location of Rio Grande (river). Dotted arrow indicates interpreted mantle upwelling. Black dashed line is crust-mantle boundary estimate from Shen et al. (2013). Location of Raton-Clayton volcanic field (RCVF) projected onto profile. LCC = lower crustal conductor; MCC = midcrustal conductor (black rectangle); CP = Colorado plateau. Geographic features: SdC = Sangre de Cristo Mountains, SJB = San Juan Basin, SLB = San Luis Basin, TM = Tusas Mountains. See Figure 2 for spatial correlation between MCC and Embudo fault zone.

models had to be exceptionally more complex than the anisotropic models. Model roughness, defined as the difference in resistivity values of each finite element relative to the adjacent elements, summed and averaged over the entire model space, can be used to quantify the differences in model complexity. For example, model roughness for the north central rift was 56 for the anisotropic model compared to 86 for the isotropic model based on the same data. In an effort to avoid overstating our model resolution, we prefer to interpret the simplest model that fits the data. In this case that model was the anisotropic inversion result.

Our preference for the anisotropic inversion result is thus informed by (1) ability to fit a slightly lower RMS target value, (2) a smoother model that fits the data equally well, (3) strong resemblance to an anisotropic signature described in Heise and Pous (2001) for a similar modeling approach, and (4) a lack of convincing evidence in the data for a series of isolated, laterally distributed conductors in the lower crust. We are not the first to suggest that the lower crust beneath the Rio Grande rift is anisotropic. Fu and Li (2015) observe radial anisotropy anomalies in the shear wave velocity structure beneath the Taos Plateau and many of the young volcanic centers of the rift. The interpretation of this seismic anisotropy and its implications for the resistivity structure are discussed below.

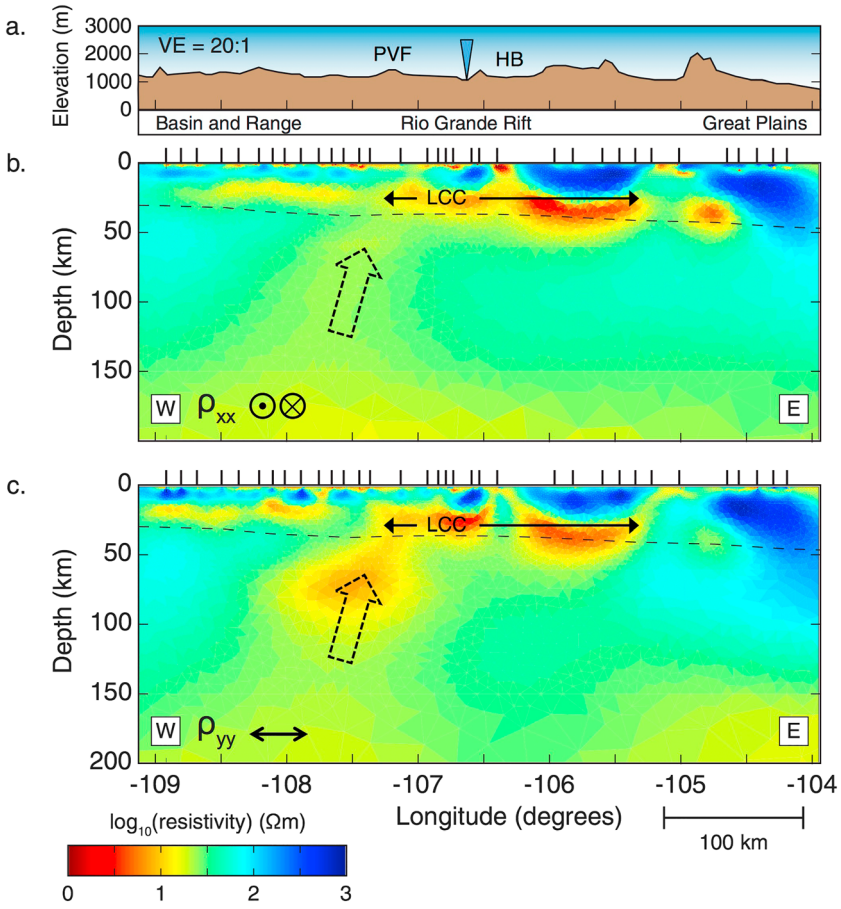

Figure 6. Anisotropic electrical resistivity model for southern rift. Includes (a) topography, (b) ρ_{xx} model, electrical resistivity structure sensed by north-south electric fields (parallel to the rift axis) and (c) ρ_{yy} model, electrical resistivity structure sensed by east-west electric fields (perpendicular to rift axis). Additional labels as in Figure 5. Midcrustal conductor is not present in the southern rift. PVF = Potrillo volcanic field, HB = Hueco Basin.

3.2. North Central Rift Structure

In general, the 2-D anisotropic resistivity model of the north central rift (Figure 5) is characterized by high-resistivity upper crust to depths of 15–25 km, a low-resistivity middle to lower crust beneath the rift axis extending laterally beneath both the Colorado Plateau and Great Plains, and a steep lateral increase in upper mantle resistivity from west to east across the Rocky Mountain front (longitude = 105°W). Additionally, there is a thin veneer of high conductivity in the uppermost crust that correlates well with surface geology, most notably the San Juan Basin (108 to 106°30′W) and the major rift basin at this latitude, the San Luis Basin (centered at 105°45′W).

The middle to lower crust of the north central rift exhibits the most pronounced anisotropic structure of either profile. The lower crust (depths > 25 km) is characterized by a broad zone (~200-km wide) of low resistivity that is either isotropic or slightly anisotropic. Meanwhile, there is a strong midcrustal conductor (MCC, depth of ~12 km) apparent in the ρ_{yy} model that is not observed in the ρ_{xx} model. The change in anisotropy between the middle and lower crust suggests that two distinct conductivity mechanisms or structural fabrics are required to fully explain these two high-conductivity anomalies in the crust.

Detailed resistivity structure of the upper mantle (depths > 45 km, Shen et al., 2013) beneath the north central rift is difficult to resolve owing to the masking effect of high crustal conductivity. We observe that the mantle exhibits relatively low resistivity (10–100 Ωm) west of the Rocky Mountain front and higher

resistivities (100–1,000 Ωm) beneath the Great Plains. The lowest mantle resistivities (10 Ωm) are found directly beneath the rift axis in the ρ_{xx} model (Figure 5b). The regional trend of eastward increasing upper mantle resistivity is interrupted in the ρ_{yy} model by a vertical resistive feature at approximately 106°W. Given the exceptionally low resistivity of the middle crust directly above it, we interpret this feature as a "resistive shadow" indicating a region to which our modeling approach is largely insensitive. The resistivity of the resistive shadow is relatively unchanged from the starting model (80 Ωm half-space for this profile). Interestingly, the lower crustal conductor (LCC) at this latitude appears to be wider than the region of enhanced conductivity in the upper mantle, especially beneath the Great Plains, where the LCC extends eastward above resistive mantle from 105° to 104°W.

3.3. Southern Rift Structure

In general, the crustal resistivity structure of the southern rift can be divided into three broadly similar vertical sections along the profile. The first, from the western edge of the model to 107°30′W, is characterized by a resistive upper crust and moderately conductive lower crust. The second, from 107°30′W to 104°30′W, exhibits a highly variable upper crust and an extremely low-resistivity lower crust (LCC, Figure 6). The third section, from 104°30′W to the eastern edge of the profile, is highly resistive throughout the entire crustal column, with the marginal exception of a thin veneer of low resistivity in the near surface.

A near-surface conductor east of the rift axis (106°30′W, Figure 6b) exhibits the strongest degree of anisotropy of any feature in the southern rift model. This conductor is the Hueco Basin, a several-kilometer-deep sedimentary basin elongated parallel to the rift axis. Sedimentary units within the Hueco Basin are presumed to be isotropically conductive, yet the resistivity models show conductivity enhanced parallel to the rift axis (i.e., north-south). This apparent anisotropy in the basin resembles a 2-D inverse response to 3-D structure that intersects the model profile but is finite in length off profile (Siripunvaraporn et al., 2005). The imaged anisotropic response of this basin highlights both a limitation and advantage of 2-D anisotropic inversion. While the elongate 3-D geometry of the basin cannot be recovered within a 2-D model, the incorporation of anisotropy permits the inversion to better fit the measured data. The Hueco Basin is one of the few regions in either profile for which the anisotropic modeling provides a quantitatively superior data misfit (see supporting information).

Two other regions of high anisotropy can be found in the lower crust east of 107°W along the southern rift profile. The more pronounced of the two is a region directly beneath the Hueco Basin, which is almost 10 times more conductive in the rift-parallel direction compared to the rift-perpendicular resistivity. The second lesser anisotropic anomaly, located at ~105°W, is enhanced in the same direction (north–south) but to a much lesser degree (factor of 3–5 anisotropy).

The LCC appears to shallow beneath, and in the case of the ρ_{yy} model connect with, the near-surface low-resistivity anomaly associated with the Hueco Basin at ~106°30′W (Figure 6). We consider this conductive connection to be an artifact of the inversion, specifically due to regularization which favors smoothly varying resistivity structure. The extremely low resistivity of the Hueco Basin atop a moderately resistive upper crust is likely difficult for the inversion to accommodate without permitting a tear in the model smoothness at the level of the basement-sediment contact. Thus, the inversion will bring the LCC up in the section so as to minimize vertical gradients in resistivity structure. Presumably, were this connectivity a real feature, it would represent a vertical migration of some deep-sourced conductive fluid, most likely partial melt or saline brines, into the Hueco Basin from greater depths. While there is significant evidence in New Mexico of deep-sourced fluid and gas mixtures using rift-related faults as conduits to reach the surface (e.g., Priewisch et al., 2014), there is no evidence of this process occurring in the area where we image the conductive conduit. Furthermore, the Hueco Basin lacks any active geothermal activity or Quaternary volcanism that would facilitate a fluid supply to the shallow crust.

The mantle beneath the southern rift is in general moderately resistive (30–100 Ωm), with the exception of a region of high conductivity centered on 107°30′W. This zone of high conductivity is anisotropic, with conductivity enhanced perpendicular to the rift axis and appears to connect with the LCC at a lateral transition in crustal structure. The upper mantle becomes more resistive (100–300 Ωm) at either end of the profile; this is more pronounced in the rift-perpendicular model (Figure 6c).

4. Discussion

4.1. Upper Crust

The upper crustal resistivity structure along both profiles (0- to 15-km depth) is dominated by conductive sedimentary basins and, to a lesser extent, resistive Precambrian rocks uplifted during the Laramide orogeny. In northern New Mexico, the upper crust is resistive beneath two prominent basement-cored uplifts that bound the Rio Grande rift, the Tusas Mountains to the west and the Sangre de Cristo Mountains to the east. Between the two uplifts, the San Luis Basin appears as a conductive unit in the near surface. To the west, the San Juan Basin, a package of Cretaceous-age marine shale, appears as a broad, near-surface conductor. To the east, a thin veneer of Mesozoic sedimentary units is imaged as discrete conductive anomalies beneath each station. These discrete anomalies are more than likely sampling a laterally contiguous package of conductive sedimentary rocks east of the Sangre de Cristo range, but the wider station spacing along this portion of the profile limits the ability of the inversion to resolve a thin, continuous conductor so close to the surface.

Along the southern profile, the upper crust is dominated by sedimentary basin structures that appear to have enhanced conductivity parallel to the rift axis (i.e., $\rho_{xx} < \rho_{yy}$). The location of these conductors correlates with the surface geology, that is, high conductivity is imaged beneath sedimentary cover and absent beneath exposed bedrock, as well as the seismic velocity structure imaged by the active-source seismic experiment of Averill and Miller (2013).

The midcrustal conductor imaged beneath the north central rift (MCC, Figure 5c, depth of ~12 km in 40-km crust) does not have an immediately obvious interpretation. Geographically, the MCC is located northeast of the Jemez volcanic field (JVF), due north of the EFZ (Bauer et al., 2016), and just south of the Tusas Mountains uplift. When projected vertically to the surface, the MCC is bounded to the west by the Cañones fault, the structural boundary between the Rio Grande rift and the Colorado Plateau, and to the east by the Rio Grande. It is unlikely that the MCC is related to magmatic activity within the rift. Based on the anisotropy of the anomaly observed in Figure 5 (i.e., $\rho_{yy} < \rho_{xx}$), it appears that electric currents preferentially flow through the MCC in an east-west direction. Oddly, this is perpendicular to the rift axis, the predominant direction of electrical anisotropy observed in the lower crust and the predominant direction of anisotropy proposed by Fu and Li (2015) for this region of north central New Mexico. Furthermore, there is no correlation between the location of the MCC at depth and volcanic activity at the surface, as it seems to straddle the western margin of the Taos Plateau volcanic field. Other volcanic loci along the Jemez lineament (i.e., the Valles caldera) are too far away (several skin depths at even the longest periods) to have much influence on the MT data that contribute to this portion of the resistivity model.

A possible interpretation of the MCC is that offline 3-D resistivity structure is projecting onto our 2-D profile (Siripunvaraporn et al., 2005; Wannamaker et al., 1984). The EFZ (Figure 2), an ENE-WSW trending strike-slip fault that serves as the northwestern margin of the Española Basin of the Rio Grande rift, may be capable of producing such an anomaly. Fault damage zones are generally conductive features of the upper crust, as they are characterized by enhanced porosity and/or permeability, often contain clay minerals, and serve as conduits for groundwater. The trend of the EFZ is subparallel to the trace of our profile, consistent with the observation that conductivity in the MCC is enhanced in an east-west direction. The east-west extent of the EFZ projected northward onto our profile is consistent with the lateral extent of the MCC in the midcrust (Figure 2). One challenge to this interpretation is that the MCC in Figure 5c is confined to depths > 12 km with very resistive crust (>1,000 Ωm) directly above it, yet we would expect the enhanced conductivity associated with a fault damage zone to extend to the near surface. This observation is actually consistent with the interpretation that we are imaging an offline conductor. The high-frequency MT data at stations directly above the MCC anomaly would not sense the offline conductor so long as the skin depth at those frequencies is less than the lateral separation between the EFZ and our profile. Thus, we would not expect these stations to sense a conductive anomaly until later periods that subsequently correspond to deeper regions of the model when inverted. Close examination of the MCC in Figure 5c reveals that it shallows near 106°W, the longitude at which the surface trace of the EFZ comes closest to piercing our profile (Figure 2).

While we can speculate qualitatively on the degree to which off-profile structure influences our 2-D anisotropic resistivity model, characterization of the upper crustal resistivity structure in the vicinity of the EFZ likely requires full 3-D modeling informed by a much denser array of MT stations than we have available

to us at this time. This does not detract from our ability to interpret the remainder of our model, especially in the context of lithosphere scale resistivity structure and the broader tectonic implications of those features.

4.2. Lower Crust

The LCC that we image at depths >20 km beneath both profiles is broad (~200-km wide), highly conductive (<20 Ωm), and exhibits enhanced conductivity in a direction parallel or subparallel to the axis of the Rio Grande rift. With a top at 20- to 25-km depth across most of our profile and a conductance of 1000–2000 S, we are confident in suggesting that this is the same crustal conductor originally observed by Hermance and Pedersen (1980). We also note that this conductor is remarkably similar in geometry (i.e., depth and lateral extent) and conductance (see Figure S4) to the LCC imaged beneath the northern Rio Grande rift and southern Rocky Mountains in Colorado by Feucht et al. (2017).

Electromagnetic geophysical studies of the rift (e.g., Jiracek et al., 1983) suggest that this conductor may be explained as free saline fluid. A large volume of interconnected, ponded fluid residing in the midcrust requires both a source of free saline fluids and a means by which to retain buoyant and reactive free fluids in equilibrium at depth. Crustal fluids in an active tectonic environment are not unusual (e.g., Becken et al., 2011; Li et al., 2003; Wannamaker et al., 2008, 2014). In the case of the lower crust beneath the Rio Grande rift, the recent introduction, or continued supply, of partial melt into the crustal column could produce free saline fluid detectable by geophysical observations. Evidence of recent injection of magma into the crust includes both young volcanic eruptions in and around the rift and present-day crustal magma storage in the JVF (Steck et al., 1998) and the Socorro magma body (Rinehart et al., 1979). As this melt cools, exsolved fluids are released into the surrounding crust. If hydrated mantle lithosphere and hydrous metamorphic minerals are present prior to melting this increases the availability of free saline fluids as these hydrous phases produce wetter melts that would exsolve more fluid upon cooling (Jahns, 1982).

Retention of free saline fluids at midcrustal depths can be accomplished in a variety of ways. Metamorphic reactions at the 300–400 °C isotherm may precipitate silica and other minerals out of crustal fluids, reducing permeability and inhibiting fluid migration upward (e.g., Hyndman & Shearer, 1989). Ductile shear zones in the middle crust may also produce a zone of structural impermeability. Seismic reflection studies performed by COCORP in the Albuquerque Basin in the north central Rio Grande rift found detachment faults in the midcrust beneath the basin, suggesting that high-angle, basin bounding normal faults shallow into listric faults at depths of ~15 km (de Voogd et al., 1988). Averill and Miller (2013) advocated for the existence of similar listric-type faults in the southern rift west of the Rio Grande based on their interpretation of seismic tomography from an active-source experiment. Low-angle listric faults at or near the brittle-ductile transition could manifest as impermeable shear zones, which could trap and concentrate upward migrating free saline fluids as they ascend the crustal column.

One feature of our results that was not considered in previous interpretations of the LCC and may assist in differentiating partial melt from saline fluid is the anisotropic behavior of the conductivity anomaly. Conductivity enhanced in the ρ_{xx} model relative the ρ_{yy} model, as observed for the LCCs in both Figures 5 and 6, implies a structural grain or fabric to the resistivity structure that preferentially channels horizontal electric current in the north-south direction, parallel to the rift axis. Melt filled lenses (i.e., magmatic dykes) injected into the lower crust during east-west extension would manifest electrically as rift-parallel conductive pathways, at least until the melt therein cools or is exhumed in volcanic eruptions. The idea that melt is present in the crust beneath New Mexico is supported by anisotropic shear wave models (Fu & Li, 2015), the imaging of crustal magma chambers beneath the JVF and the Socorro magma body, and the composition of lavas from recent volcanism along the Jemez lineament in north-central New Mexico. Lavas from the Taos Plateau volcanic field, Ocate volcanic field and Raton-Clayton volcanic field all exhibit geochemical characteristics of crustal contamination, implying that these magmas spent significant time equilibrating in the crust prior to erupting (e.g., Nielsen & Dungan, 1985).

How do we differentiate partial melt from saline fluids in a tectonic environment that may produce both types of fluid? Seismic tomography (Fu & Li, 2015) and heat flow modeling (Decker et al., 1988) suggest that the crust is elevated in temperature beneath the rift. In an otherwise tectonically stable region this would favor the melt interpretation, with the implication that elevated heat flow and slow velocities are a product of melt injection. However, within the Rio Grande rift, the close proximity of a hot upper mantle to the base

of an attenuated lithosphere could produce these same observations without the need for melt. Modeling heat flow data in the rift with the assumption of a conductive geotherm produces temperatures above the solidus at depths above the Moho (Decker et al., 1988), suggesting extremely high volumes of partial melt are present in the crust or more likely, there has been advective heat transfer into the crust from the mantle. Seismic attenuation in the crust beneath the rift is high (Phillips et al., 2014), which would support the presence of melt if we assume intrinsic attenuation rather than scattering attenuation (e.g., heavily fractured rock dispersing seismic energy). However, a vast network of rift-aligned cracks filled with saline brine rather than melt would also enhance attenuation due to both modification of bulk intrinsic physical properties and wave scattering.

In summary, it is difficult to differentiate between partial melt and free saline fluids in a tectonic environment in which both are reasonable (e.g., Feucht et al., 2017; Li et al., 2003). That the electrical conductivity of the lower crustal anomaly appears to be enhanced in the direction parallel to the rift axis in the anisotropic model (e.g., Figure 5b) suggests the presence of partial melt within a network of vertical, rift-parallel lenses. Fu and Li (2015) use a similar model to explain negative radial anisotropy in shear wave velocity measurements beneath the Taos Plateau in north central New Mexico. The apparent necessity of partial melt does not preclude the presence of free saline fluid occupying grain boundary spaces in the deep crust. That the LCC is only moderately anisotropic suggests that some largely isotropic conductivity mechanism, be it partial melt uniformly distributed throughout the lower crustal, horizontal melt-filled lenses (i.e., magmatic sills), or saline fluids ponded in the middle crust, contributes to the observed high conductivity. This two-phase interpretation that favors the presence of both free saline fluids and partial melt is similar to the conductivity mechanism invoked by Wannamaker et al. (2008) to explain high crustal conductivity at the Great Basin-Colorado Plateau transition in central Utah. Based on the metamorphic grade of the crust, the local geotherm, and the stability criteria of different fluids, Wannamaker et al. favors a model in which partial melt occupies the deep crust and free saline-fluids are more prevalent in the midcrust.

Quantitative estimates of fluid volumes and partial melt fraction derived from regularized inversion of MT data can at best provide bounds on the possible fluid content of the lower crust. For estimates of fluid content and possible end-member fluid compositions (i.e., partial melt vs free saline fluid), we appeal to the analysis of Feucht et al. (2017) and their detailed examination of the LCC imaged beneath the northern Rio Grande rift in Colorado. We justify this comparison by noting the similarities in geophysical properties and tectonic setting of the two LCCs, both of which are interpreted to have been emplaced in response to east-west extension of the lithosphere along the western margin of the Great Plains in the late-Cenozoic. In Feucht et al. (2017), high electrical conductivity beneath central Colorado is explained by, alternatively, 7–15% basaltic partial melt distributed from the top of the conductor to the crust-mantle boundary (higher concentrations if partial melt is hybridized or nonuniformly distributed), free saline brine in volumes as low as 0.7 vol %, or some combination of the two conductive phases, with free saline fluid more likely to be stable near the middle crust. We favor the two-phase conductor model, with saline fluid concentrated in the midcrust, given that crustal temperatures at depths corresponding to the top of the LCC are insufficient to support melting (Decker et al., 1988).

4.3. Upper Mantle

Based on the high resistivity values imaged in the upper mantle east of 105°W and the spatial correlation with a similarly sharp increase in seismic velocity observed in teleseismic tomography studies (e.g., Shen et al., 2013), we conclude that the subcontinental lithospheric mantle beneath the western Great Plains in northern New Mexico is likely cold and relatively water-free. This is in contrast to both high conductivity beneath the westernmost Great Plains observed farther north in Colorado (Feucht et al., 2017) and the only moderately resistive mantle imaged beneath the Colorado Plateau on the western side of the north central rift profile. Interestingly, the LCC along both the north central and southern rift profiles extends beneath the westernmost Great Plains (Figures 5 and 6). The presence of a midcrustal zone of moderately high conductivity beneath the Great Plains has been known for some time (e.g., Landisman & Chaipayungpin, 1977), although Feucht et al. (2017) failed to image any low resistivity zone in the lower crust beneath eastern Colorado. That electrically conductive lower crust is present above a resistive upper mantle (as in the north central profile, longitude 105–104°W, Figure 5b) suggests some mechanism for supplying partial melt through stable lithosphere. Vertical transport of fluids and/or melt through seemingly tectonically stable

lithosphere is not unreasonable, as the Raton-Clayton volcanic field of northeastern New Mexico (located approximately 70 km north of our profile and more than 100 km east of the rift, see Figures 1 and 2) has generated Holocene cinder cones and lava flows despite being underlain by lithosphere that is interpreted in seismic tomographic studies to be cold and dry.

An alternative interpretation of the resistive upper mantle beneath the north central rift is that the mantle lithosphere is depleted in melt and volatiles following the fluxing of partial melt into the lower crust. A similar interpretation has been invoked to explain relatively resistive upper mantle beneath the Great Basin-Colorado Plateau transition zone in central Utah (Wannamaker et al., 2008). Volcanism in New Mexico, especially in the late Cenozoic, has been concentrated along the Jemez lineament, which cuts across the north central portion of the Rio Grande rift and trends subparallel to our northern profile (Figure 2a). That the mantle lithosphere beneath the eastern margin of the rift appears to be less resistive to the south (this study) and the north (Feucht et al., 2017) may indicate that on a regional scale, a hydrated and/or melted upper mantle is the norm rather than the exception in the tectonic regime of the Rio Grande rift and western Great Plains. In this scenario, less resistive portions of the upper mantle beneath the north central rift are regions that have either retained partial melt over geologic time or have been subjected to more recent episodes of upwelling and decompression melting.

The highly anisotropic conductivity anomaly west of the Great Plains lithosphere beneath the north central rift (conductivity enhanced parallel to the rift axis, see Figure 5b) provides insight into the mantle processes that have led to the presence of fluids in the lower crust. One hypothesis is that lithospheric extension in the Rio Grande rift has allowed for adiabatic upwelling and melting of the upper mantle, producing basaltic melts that are imaged here as zones of high electrical conductivity. That the electrical anisotropy of this feature is enhanced rift-parallel (i.e., enhanced in the ρ_{xx} model) suggests that the upwelling is related to the regional extensional stress regime (minimum compressive stress oriented north–south). Basaltic melt is negatively buoyant in the mantle and would tend to rise, pool at the base of the crust and infiltrate the lower crust, where it would cool, releasing saline fluids. These saline fluids would continue to rise buoyantly through the lower crust but may stall in the midcrust under the appropriate conditions. It is likely that the imaged LCC is a combination of basaltic melt originating from the mantle, anatectic silicic melts produced from the introduction of heat and volatiles to the lower crust, and saline fluids released when these melts cool.

The most prominent feature of upper mantle resistivity structure beneath the southern rift is an anisotropic conductor located directly beneath the transition between the Rio Grande rift and the Basin and Range (107.5°W in Figure 6c). Similar to the anisotropic conductor beneath the north central rift, we interpret this feature as an indication of adiabatic upwelling and decompression melting of the mantle to produce basaltic melts that then infiltrate the lower crust. That the anisotropy of this feature exhibits a significant east–west orientation (i.e., electrical conductivity in this part of the model appears to be enhanced in Figure 6c relative to Figure 6b) suggests that there could be a component of rift perpendicular flow as well.

4.4. Synthesis

Figure 7 is an interpretive diagram highlighting the various features of our anisotropic resistivity models of the Rio Grande rift. A key feature of our interpretation is the differentiation of the Rio Grande rift from adjacent tectonic provinces based on the geophysical properties of the crust and upper mantle. For example, the eastern boundary of the Rio Grande rift in southern New Mexico may be alternatively defined in terms of structure, geology, or geophysical properties. Structurally and geologically, the boundary would fall on the eastern margin of the Hueco Basin (~106°W), which contains the easternmost exposure of synrift sediments (Figure 1) and is bounded by high-angle normal faults active in the Quaternary (Seager, 1980). If, however, the extent of the LCC reflects that of rift-related lithospheric modification, we should place the eastern rift boundary about 100 km farther east.

Farther west along the southern profile, we see another delineation between tectonic provinces in the form of a distinct change in crustal resistivity structure at approximately 107.5°W. West of this boundary lies the relatively dormant Southern Basin and Range province, with lower crustal conductivity markedly lower than that of the Rio Grande rift to the east (see supporting information Figure S4). Interestingly, this boundary coincides with the center of the most pronounced mantle conductor in the southern rift as well as the

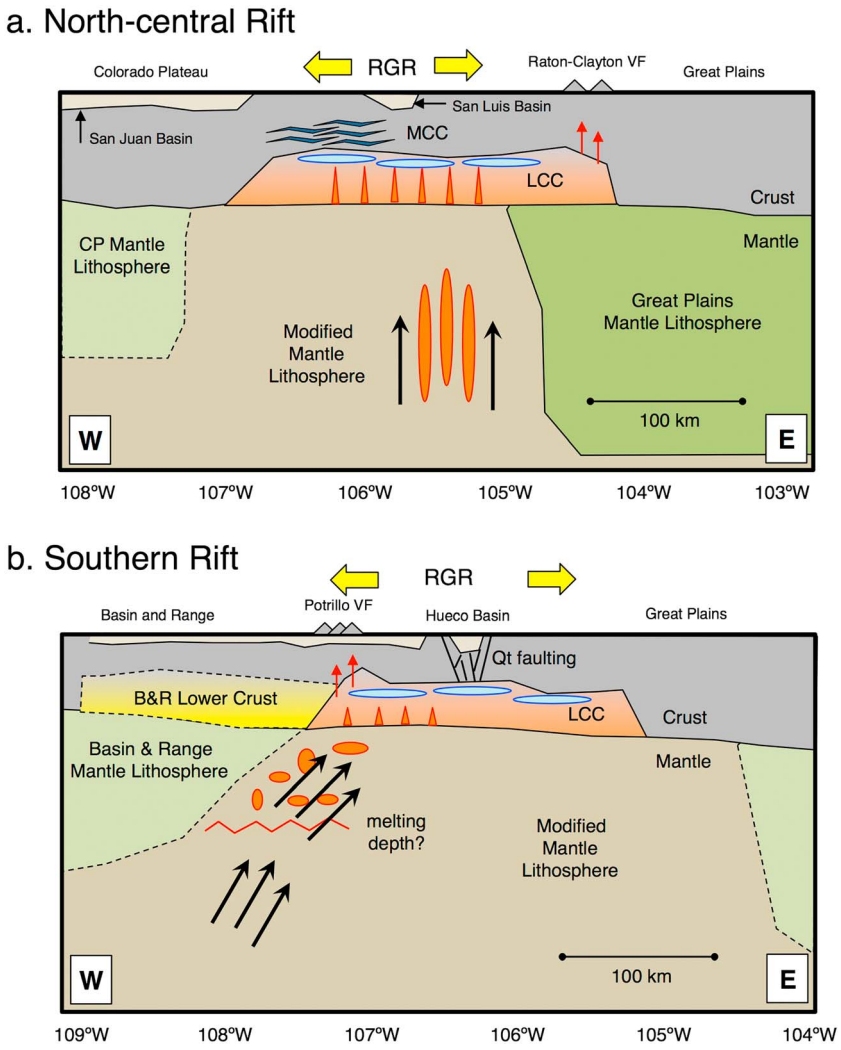

Figure 7. Interpretation of anisotropic electrical resistivity models for (a) the north central Rio Grande rift and (b) the southern rift. Compare to resistivity models, Figures 5 and 6. Both profiles centered on rift axis showing interpretative cross sections approximately 400-km wide and 150-km deep. Interpreted upward mantle flow indicated by groups of black arrows. Lithosphere-asthenosphere boundary not shown and not well defined in resistivity models. Lower crustal conductor (LCC) interpreted as combination of axis-parallel melt-filled dikes (orange ellipses) and ponded saline fluids (blue ellipses) in the middle crust. Midcrustal conductor (MCC) in (a) interpreted as northward projection of the Embudo fault zone (wavy lines). Red arrows indicate supply of melt to Potrillo volcanic field in (b) and Raton-Clayton volcanic field in (a). Orange blobs indicate decompression melting in upper mantle. Yellow arrows indicate east-west oriented extension away from rift axis.

Quaternary Potrillo volcanic field, one of the more significant volcanic centers in the rift outside the Jemez lineament. That these features are vertically aligned suggests a connection between recent decompression melting in the upper mantle and young volcanics along the rift.

In the north central rift, the Great Plains are characterized by a resistive crust and highly resistive mantle lithosphere east of 105°W. The lithospheric boundary between the Colorado Plateau and the rift to the west is less distinct, but we argue exists just east of 107°W based on a lack of LCC (this happens to coincide with the topographic boundary of the Colorado Plateau, the Cañones fault scarp near Abiquiu, New Mexico (Baldridge et al., 1994)).

Another key feature of our interpretation is that, despite significant variability in inherited lithospheric structure, crustal thickness, width of extension, and surface geology along the axis of the Rio Grande rift, the resistivity structure of the lower crust in this tectonic regime appears to be remarkably uniform

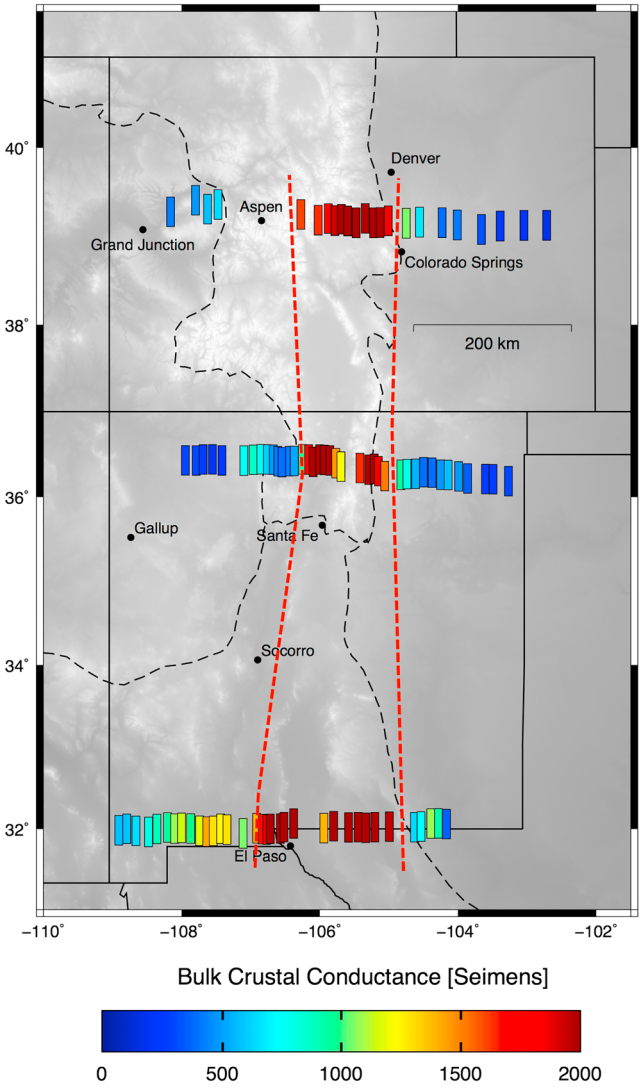

Figure 8. Bulk lower crustal conductance in map view. Conductance is conductivity thickness product integrated over the lower crust (15- to 50-km depth for northern and north central rift; 15–40 km for southern rift) and averaged between the ρ_{xx} and ρ_{yy} resistivity models. Conductance for the northern rift comes from 2-D anisotropic resistivity models in Feucht et al. (2017). Black dashed lines are physiographic provinces (Fenneman, 1946); red dashed lines denote mean crustal conductance above 1,500 S (contour chosen to match minimum conductance of lower crustal conductor originally modeled by Hermance & Pedersen, 1980). Note the uniform width of the crustal-conductance anomaly along the rift axis. Background shading is elevation.

(Figure 8). The low resistivity zone that we image in this study has been observed previously in regional (Feucht et al., 2017) and local (Hermance & Pedersen, 1980; Nettleton, 1997) studies of the Rio Grande rift conductivity structure. The addition of the two wide-aperture, deep sensing MT profiles presented here allows us to put these previous observations into a larger tectonic context. Parsimony suggests that a similar mechanism of lithospheric modification, active along the entire axis of the rift from northern Mexico to central Colorado, would produce a similar signature in the electrical resistivity structure observed by MT.

The results of 2-D anisotropic modeling of MT data along our two profiles support the hypothesis that vertically aligned lenses of mantle-sourced basaltic melt have infiltrated the lower crust beneath the Rio Grande rift in New Mexico. Furthermore, enhanced electrical conductivity in the upper mantle suggests that some fraction of partial melt exists in the mantle today. Given the tectonic context, the genesis of melt is likely decompression melting that occurs in adiabatic upwelling of the mantle lithosphere. The larger tectonic mechanism driving adiabatic upwelling is not readily apparent from the resistivity models. Geodynamic modeling by van Wijk et al. (2010) and seismic tomography from the LA RISTRA experiment (e.g., Gao et al., 2004) suggests that lithospheric upwelling beneath New Mexico is a result of edge-driven convection, initiated by differential lithospheric thickness along the western margin of the Great Plains at the end of the Laramide orogeny. That the surface expression of the rift widens to the south (Figure 1) despite the observation that the rift appears to have opened simultaneously along its entire length (Landman & Flowers, 2013) suggests that the Colorado Plateau is rotating clockwise away from the Great Plains. Lithospheric extension occurring in the wake of the rotating block would also produce adiabatic mantle upwelling. Edge-driven convection and large-scale plate motions are not mutually exclusive, and it is likely that both contribute to upper mantle convection beneath the Rio Grande rift (Ballmer et al., 2015).

Our MT observations provide a rough control on the timing of these tectonic processes in that the conductive phases we invoke to explain the electrical resistivity anomalies in the modern-day lithosphere are transitory over geologic time scales. Partial melt is only electrically conductive so long as it has not frozen, and free saline fluids are only conductive so long as they have not been absorbed into the surrounding rock via metamorphic reactions. Given the geologically short timescales over which free saline fluid is stable in the lower crust and partial melt cools following injection, the MT results suggest that there has been a relatively recent supply of melt, and subsequent exsolved fluids to the lower crust in New Mexico. This is consistent with the assertions of Berglund et al. (2012) and Nakai et al. (2017) that the rift is still very much an active tectonic feature of the western United States.

5. Conclusions

Inverting broadband and long-period MT data along two wide-aperture, high-resolution profiles under the assumption of electrical anisotropy reveals a middle to LCC beneath the Rio Grande rift in New Mexico. By interpreting this conductor in the context of other geologic and geophysical data as well as the broader tectonic setting, we can better constrain the possible conductivity mechanisms and tectonic implications of this geophysical anomaly. Our models show that the lateral extent of the LCC exceeds the surface expression of recent rifting, encroaching eastward into the Great Plains, and westward into the Colorado Plateau and Basin and Range. The uniformity in geometry, depth, and conductivity of the LCC along the entire rift

axis suggests it is a characteristic feature of the Rio Grande rift. The feature is sufficiently distinct in our resistivity models to provide a novel, geophysical basis for differentiating the rift from the surrounding tectonic provinces. The high conductance of the LCC and the tectonic history of the region point to a fluid source, that is, saline brines and/or partial melt, rather than conductive mineralogy. The exception to this interpretation is the midcrustal conductor imaged beneath the western rift boundary in northern New Mexico, the interpretation of which is less obvious but may be related fault zone alteration in the upper crust. The modern-day presence of fluids in the lower crust is attributed to an influx of basaltic melt from the upper mantle, a direct consequence of adiabatic mantle upwelling and subsequent decompression melting of the continental lithosphere.

Acknowledgments
The authors thank Phil Wannamaker, Benjamin Drenth, and one anonymous reviewer for constructive comments and suggestions. The authors thank Craig Jones, Jenny Nakai, George Jiracek, Scott Baldridge, Shari Kelley, and John Ferguson for valuable discussions. We thank Kerry Key and the Seafloor Electromagnetic Methods Consortium for the use of MARE2DEM and advice on its use. Our MT data were collected over two summer field campaigns through a joint effort by the University of Colorado Boulder and the U.S. Geological Survey. Georgianna Zelenak, Daniel Zietlow, Andrew Adams, Jennifer Harding, Robert Kowalski, and Kate Selway provided significant contributions to the field effort. Instrumentation was provided by the U.S. Geological Survey in Denver, CO and by Martyn Unsworth at the University of Alberta. This work was supported by the University of Colorado Boulder Geological Sciences Department W.O. Thompson Award and Spetzler Award, the Society of Exploration Geophysicists, the Geological Society of America, and National Science Foundation grants EAR-1249669 and EAR-1053596. Additional support was provided by EarthScope (EAR-0323309). This work would not have been possible without land access granted by the National Forest Service, the State of New Mexico, the Bureau of Land Management, and several private landowners. Various maps and graphics were created using Generic Mapping Tools (Wessel & Smith, 1991). Any use of trade, firm, or product names is for descriptive purposes only and does not imply endorsement by the U.S. Government. Magnetotelluric transfer function estimates and time series used in this analysis are available through a U.S. Geological Survey data release (Feucht et al., 2018) hosted on ScienceBase (https://doi.org/10.5066/F7610XTR).

References

Aldrich, M. J. (1986). Tectonics of the Jemez lineament in the Jemez Mountains and Rio Grande rift. *Journal of Geophysical Research*, *91*(B2), 1753–1762. https://doi.org/10.1029/JB091iB02p01753

Averill, M. G., & Miller, K. C. (2013). Upper crustal structure of the southern Rio Grande rift: A composite record of rift and pre-rift tectonics. In M. R. Hudson & V. J. S. Grauch (Eds.), *New perspectives on Rio Grande rift basins: From tectonics to groundwater—Geological Society of America Special Paper 494* (pp. 463–474). Boulder, CO: Geological Society of America. https://doi.org/10.1130/2013.2494(17)

Baldridge, W. S., Bartov, Y., & Kron, A. (1983). Geologic map of the Rio Grande rift and southeastern Colorado plateau, New Mexico and Arizona (scale 1:500,000). In R. E. Riecker (Ed.), *Rio Grande Rift: Tectonics and Magmatism*. Washington, DC: American Geophysical Union.

Baldridge, W. S., Braile, L. W., Biehler, S., Jiracek, G. R., Ferguson, J. F., Hasterok, D., et al. (2012). SAGE at 30. *The Leading Edge*, *31*(6), 702–708. https://doi.org/10.1190/tle31060702.1

Baldridge, W. S., Ferguson, J. F., & Wang, B. H. (1994). The western margin of the Rio Grande rift in northern New Mexico: An aborted boundary? *Geological Society of America Bulletin*, *106*(12), 1538–1551. https://doi.org/10.1130/0016-7606(1994)106<1538:TWMOTR>2.3.CO;2

Ballmer, M. D., Conrad, C. P., Smith, E. I., & Johnsen, R. (2015). Intraplate volcanism at the edges of the Colorado plateau sustained by a combination of triggered edge-driven convection and shear-driven upwelling. *Geochemistry, Geophysics, Geosystems*, *16*, 366–379. https://doi.org/10.1002/2014GC005641

Bauer, P. W., Kelson, K. I., Grauch, V. J. S., Drenth, B. J., Johnson, P. S., Aby, S. B., & Felix, B. (2016). Geologic map and cross sections of the Embudo fault zone in the Southern Taos Valley, Taos County, New Mexico (Open-File Report 584). New Mexico Bureau of Geology and Mineral Resources.

Becken, M., Ritter, O., Bedrosian, P. A., & Weckmann, U. (2011). Correlation between deep fluids, tremor and creep along the central San Andreas fault. *Nature*, *480*(7375), 87–90. https://doi.org/10.1038/nature10609

Berglund, H. T., Sheehan, A. F., Murray, M. H., Roy, M., Lowry, A. R., Nerem, R. S., & Blume, F. (2012). Distributed deformation across the Rio Grande rift, Great Plains, and Colorado plateau. *Geology*, *40*(1), 23–26. https://doi.org/10.1130/G32418.1

Biehler, S., Ferguson, J., Baldridge, W. S., Jiracek, G. R., Aldern, J. L., Martinez, M., et al. (1991). A geophysical model of the Española Basin, Rio Grande rift, New Mexico. *Geophysics*, *56*(3), 340–353. https://doi.org/10.1190/1.1443048

Caldwell, T. G., Bibby, H. M., & Brown, C. (2004). The magnetotelluric phase tensor. *Geophysical Journal International*, *158*(2), 457–469. https://doi.org/10.1111/j.1365-246X.2004.02281.x

Chapin, C. E., & Cather, S. M. (1994). Tectonic setting of the axial basins of the northern and central Rio Grande rift. In G. R. Keller, & S. M. Cather (Eds.), *Basins of the Rio Grande rift: Structure, stratigraphy, and tectonic setting—Geological Society of America Special Paper 291*, (pp. 5–26). Boulder, CO: Geological Society of America. https://doi.org/10.1130/SPE291-p5

Constable, S., Shankland, T. J., & Duba, A. (1992). The electrical conductivity of an isotropic olivine mantle. *Journal of Geophysical Research*, *97*(B3), 3397–3404. https://doi.org/10.1029/91JB02453

Cosca, M. A., Thompson, R. A., Lee, J. P., Turner, K. J., Neymark, L. A., & Premo, W. R. (2014). $^{40}Ar/^{39}Ar$ geochronology, isotope geochemistry (Sr, Nd, Pb), and petrology of alkaline lavas near Yampa, Colorado: Migration of alkaline volcanism and evolution of the northern Rio Grande rift. *Geosphere*, *10*(2), 374–400. https://doi.org/10.1130/GES00921.1

Dai, L., & Karato, S. (2009). Electrical conductivity of orthopyroxene: Implications for the water content of the asthenosphere. *Proceedings of the Japan Academy Series B*, *85*(10), 466–475. https://doi.org/10.2183/pjab.85.466

de Voogd, B., Serpa, L., & Brown, L. (1988). Crustal extension and magmatic processes: COCORP profiles from Death Valley and the Rio Grande rift. *Geological Society of America Bulletin*, *100*(10), 1550–1567. https://doi.org/10.1130/0016-7606(1988)100<1550:CEAMPC>2.3.CO;2

Decker, E. R., Heasler, H. P., Buelow, K. L., Baker, K. H., & Hallin, J. S. (1988). Significance of past and recent heat-flow and radioactivity studies in the Southern Rocky Mountains region. *Geological Society of America Bulletin*, *100*(12), 1851–1885. https://doi.org/10.1130/0016-7606(1988)100<1851:SOPARH>2.3.CO;2

DeGroot-Hedlin, C., & Constable, S. (1990). Occam's inversion to generate smooth, two-dimensional models from magnetotelluric data. *Geophysics*, *55*(12), 1613–1624. https://doi.org/10.1190/1.1442813

Egbert, G. D. (1997). Robust multiple-station magnetotelluric data processing. *Geophysical Journal International*, *130*(2), 475–496. https://doi.org/10.1111/j.1365-246X.1997.tb05663.x

Fenneman, N. M. (1946). *Physical divisions of the United States (scale 1:7,500,000)*. Reston, VA: U.S. Geological Survey.

Feucht, D. W., Bedrosian, P. A., & Sheehan, A. F. (2018). Regional scale magnetotelluric data from the Rio Grande rift and southern Rocky Mountains: U.S. Geological Survey Data Release. https://doi.org/10.5066/F7610XTR

Feucht, D. W., Sheehan, A. F., & Bedrosian, P. A. (2017). Magnetotelluric imaging of lower crustal melt and lithospheric hydration in the Rocky Mountain front transition zone, Colorado, USA. *Journal of Geophysical Research: Solid Earth*, *122*, 9489–9510. https://doi.org/10.1002/2017JB014474

Folsom, M., Pepin, J., Peacock, J., Person, M., Kelley, S., & Love, D. (2017). *3D inverse models of magnetotelluric data in the Central Rio Grande rift illuminate rift basin geometry and possible interactions between deep brines and surface waters*. Paper presented at New Mexico Geological Society Annual Spring Meeting, Socorro, New Mexico, USA.

Fu, Y. V., & Li, A. (2015). Crustal shear wave velocity and radial anisotropy beneath the Rio Grande rift from ambient noise tomography. *Journal of Geophysical Research: Solid Earth*, *120*, 1005–1019. https://doi.org/10.1002/2014JB011602

Gamble, T. D., Goubau, W. M., & Clarke, J. (1979). Magnetotellurics with a remote magnetic reference. *Geophysics*, *44*(1), 53–68. https://doi.org/10.1190/1.1440923

Gao, W., Grand, S. P., Baldridge, W. S., Wilson, D., West, M., Ni, J. F., & Aster, R. (2004). Upper mantle convection beneath the central Rio Grande rift imaged by *P* and *S* wave tomography. *Journal of Geophysical Research*, *109*, B03305. https://doi.org/10.1029/2003JB002743

Gilbert, H. (2012). Crustal structure and signatures of recent tectonism as influenced by ancient terranes in the western United States. *Geosphere*, *8*(1), 141–157. https://doi.org/10.1130/GES00720.1

Gile, L. (1987). A pedogenic chronology for Kilbourne Hole, southern New Mexico-II. Time of explosions and soil events before explosions. *Soil Society of America Journal*, *51*(3), 746–760. https://doi.org/10.2136/sssaj1987.03615995005100030032x

Gok, R., Ni, J. F., West, M., Sandvol, E., Wilson, D., Aster, R., et al. (2003). Shear wave splitting and mantle flow beneath LA RISTRA. *Geophysical Research Letters*, *30*(12), 1614. https://doi.org/10.1029/2002GL016616

Grauch, V. J. S., & Connell, S. D. (2013). New perspectives on the geometry of the Albuquerque Basin, Rio Grande rift, New Mexico: Insights from geophysical models of rift-fill thickness. In M. R. Hudson & V. J. S. Grauch (Eds.), *New perspectives on Rio Grande rift basins: From tectonics to groundwater: Geological Society of America Special Paper 494* (pp. 427–474). Boulder, CO: Geological Society of America. https://doi.org/10.1130/2013.2494(16)

Groom, R. W., & Bailey, R. C. (1989). Decomposition of the magnetotelluric tensors in the presence of local three-dimensional galvanic distortion. *Journal of Geophysical Research*, *94*(B2), 1913–1925. https://doi.org/10.1029/JB094iB02p01913

Heise, W., & Pous, J. (2001). Effects of anisotropy on the two-dimensional inversion procedure. *Geophysical Journal International*, *147*(3), 610–621. https://doi.org/10.1046/j.0956-540x.2001.01560.x

Hermance, J. F. (1979). *Toward assessing the geothermal potential of the Jemez Mountains volcanic complex: A telluric-magnetotelluric survey (Informal Report LA-7656-MS)*. Los Alamos, NM: Los Alamos National Laboratory.

Hermance, J. F., & Neumann, G. A. (1991). The Rio Grande rift: New electromagnetic constraints on the Socorro magma body. *Physics of the Earth and Planetary Interiors*, *66*(1-2), 101–117. https://doi.org/10.1016/0031-9201(91)90107-S

Hermance, J. F., & Pedersen, J. (1980). Deep structure of the Rio Grande rift: A magnetotelluric interpretation. *Journal of Geophysical Research*, *85*(B7), 3899–3912. https://doi.org/10.1029/JB085iB07p03899

Hyndman, R. D., & Shearer, P. M. (1989). Water in the lower continental crust: Modelling magnetotelluric and seismic reflection results. *Geophysical Journal International*, *98*(2), 343–365. https://doi.org/10.1111/j.1365-246X.1989.tb03357.x

Jahns, R. H. (1982). Internal evolution of pegmatite bodies. In P. Cerny (Ed.), *Short Course in Granitic Pegmatites in Science and Industry* (pp. 293–327). Winnipeg, MB: Mineralogical Association of Canada.

Jiracek, G. R., Gustafson, E. P., & Mitchell, P. S. (1983). Magnetotelluric results opposing magma origin of crustal conductors in the Rio Grande rift. *Tectonophysics*, *94*(1-4), 299–326. https://doi.org/10.1016/0040-1951(83)90022-7

Jiracek, G.R., Kinn, C.L., Scott, C.L., Kuykendall, M.G., Baldridge, W.S., Biehler, S., et al. (1996). Tracing crustal isotherms under the western margin of the Jemez Mountains using SAGE and industry magnetotelluric data. *New Mexico Geological Society Guidebook*. 47th conference, Jemez Mountains Region.

Keller, G. R., Khan, M. A., Morgan, P., Wendlandt, R. F., Baldridge, W. S., Olsen, K. H., et al. (1991). A comparative study of the Rio Grande and Kenya rifts. *Tectonophysics*, *197*(2-4), 355–371. https://doi.org/10.1016/0040-1951(91)90050-3

Key, K. (2016). MARE2DEM: A 2-D inversion code for controlled-source electromagnetic and magnetotelluric data. *Geophysical Journal International*, *207*(1), 571–588. https://doi.org/10.1093/gji/ggw290

Kluth, C. F., & Schaftenaar, C. H. (1994). Depth and geometry of the northern Rio Grande rift in the San Luis Basin, south-Central Colorado. In G. R. Keller & S. M. Cather (Eds.), *Basins of the Rio Grande rift: Structure, stratigraphy, and tectonic setting: Geological Society of America Special Paper 291* (pp. 27–37). Boulder, CO: Geological Society of America.

Landisman, M., & Chaipayungpin, W. (1977). First results from electrical and seismic studies of low-resistivity, low-velocity material beneath eastern Colorado. *Geophysics*, *42*(4), 804–810. https://doi.org/10.1190/1.1440748

Landman, R. L., & Flowers, R. M. (2013). (U-Th)/He thermochronologic constraints on the evolution of the northern Rio Grande rift, Gore range, Colorado, and implications for rift propagation models. *Geosphere*, *9*(1), 170–118. https://doi.org/10.1130/GES00826.1

Li, S., Unsworth, M. J., Booker, J. R., Wei, W., Tan, H., & Jones, A. G. (2003). Partial melt or aqueous fluid in the midcrust of southern Tibet? Constraints from INDEPTH magnetotelluric data. *Geophysical Journal International*, *153*(2), 289–304. https://doi.org/10.1046/j.1365-246X.2003.01850.x

Lipman, P. W., & Mehnert, H. H. (1975). Late Cenozoic basaltic volcanism and development of the Rio Grande depression in the southern Rocky Mountains. In B. F. Curtis (Ed.), *Cenozoic history of the southern Rocky Mountains: Geologic Society of America Memoir* (Vol. 144, pp. 119–154). Boulder, CO: Geological Society of America. https://doi.org/10.1130/MEM144-p119

Magnani, M. B., Miller, K. C., Levander, A., & Karlstrom, K. (2004). The Yavapai-Mazatzal boundary: A long-lived tectonic element in the lithosphere of southwestern North America. *Geological Society of America Bulletin*, *116*(9), 1137–1142. https://doi.org/10.1130/B25414.1

Nakai, J. S., Sheehan, A. F., & Bilek, S. L. (2017). Seismicity of the Rocky Mountains and Rio Grande rift from the EarthScope transportable Array and CREST temporary seismic networks, 2008–2010. *Journal of Geophysical Research: Solid Earth*, *122*, 2173–2192. https://doi.org/10.1002/2016JB013389

Nettleton, C. (1997). *Magnetotelluric modeling of the Valles caldera, New Mexico (Master's thesis)*. San Diego, CA: San Diego State University.

Nielsen, R. L., & Dungan, M. A. (1985). The petrology and geochemistry of the Ocate volcanic field, north-Central New Mexico. *Geological Society of America Bulletin*, *96*(3), 296–312. https://doi.org/10.1130/0016-7606(1985)96<296:TPAGOT>2.0.CO;2

Obrebski, M., Allen, R. M., Pollitz, F., & Hung, S.-H. (2011). Lithosphere-asthenosphere interaction beneath the western United States from the joint inversion of body-wave traveltimes and surface-wave phase velocities. *Geophysical Journal International*, *185*(2), 1003–1021. https://doi.org/10.1111/j.1365-246X.2011.04990.x

Phillips, W. S., Mayeda, K. M., & Malagnini, L. (2014). How to invert multi-band, regional phase amplitudes for 2-D attenuation and source parameters: Tests using the USArray. *Pure and Applied Geophysics*, *171*(3-5), 469–484. https://doi.org/10.1007/s00024-013-0646-1

Poe, B. T., Romano, C., Nestola, F., & Smyth, J. R. (2010). Electrical conductivity anisotropy of dry and hydrous olivine at 8 GPa. *Physics of the Earth and Planetary Interiors*, *181*(3-4), 103–111. https://doi.org/10.1016/j.pepi.2010.05.003

Priewisch, A., Crossey, L. J., Karlstrom, K. E., Polyak, V. J., Asmerom, Y., Nereson, A., & Ricketts, J. W. (2014). U-series geochronology of large-volume quaternary travertine deposits of the southeastern Colorado plateau: Evaluating episodicity and tectonic and paleohydroligc controls. *Geosphere*, *10*(2), 401–423. https://doi.org/10.1130/GES00946.1

Repasch, M., Karlstrom, K., Heizler, M., & Pecha, M. (2017). Birth and evolution of the Rio Grande fluvial system in the past 8 Ma: Progressive downward integration and the influence of tectonics, volcanism, and climate. *Earth-Science Reviews*, *168*, 113–164. https://doi.org/10.1016/j.earscirev.2017.03.003

Ricketts, J. W., Kelley, S. A., Karlstrom, K. E., Schmandt, B., Donahue, M. S., & van Wijk, J. (2015). Synchronous opening of the Rio Grande rift along its entire length at 25–10 Ma supported by apatite (U-Th)/he and fission-track thermochronology, and evaluation of possible driving mechanisms. *Geological Society of America Bulletin*, *128*(3-4), 397–424. https://doi.org/10.1130/B31223.1

Rinehart, E.J., Sanford, A.R., and Ward, R.M. (1979). Geographic extent and shape of extensive magma body at midcrustal depths in the Rio Grande rift near Socorro, New Mexico. In R. E. Riecker (Ed.), *Rio Grande Rift: Tectonics and Magmatism*. https://doi.org/10.1029/SP014p0237

Rodriguez, B. D., & Sawyer, D. A. (2013). Geophysical constraints on Rio Grande rift structure and stratigraphy from magnetotelluric models and borehole resistivity logs, northern New Mexico. In M. R. Hudson & V. J. S. Grauch (Eds.), *New perspectives on Rio Grande rift basins: From tectonics to groundwater: Geological Society of America Special Paper 494* (pp. 323–344). Boulder, CO: Geological Society of America. https://doi.org/10.1130/2013.2494(13)

Russell, L. R., & Snelson, S. (1994). Structure and tectonics of the Albuquerque basin segment of the Rio Grande rift: Insights from reflection seismic data. In G. R. Keller & S. M. Cather (Eds.), *Basins of the Rio Grande rift: Structure, stratigraphy, and tectonic setting: Geological Society of America Special Paper 291* (pp. 83–112). Boulder, CO: Geological Society of America. https://doi.org/10.1130/SPE291-p83

Schmandt, B., & Humphreys, E. (2010). Complex subduction and small-scale convection revealed by body-wave tomography of the western United States upper mantle. *Earth and Planetary Science Letters*, *297*(3-4), 435–445. https://doi.org/10.1016/j.epsl.2010.06.047

Schmandt, B., Lin, F.-C., & Karlstrom, K. E. (2015). Distinct crustal isostasy trends east and west of the Rocky Mountain front. *Geophysical Research Letters*, *42*, 10,290–10,298. https://doi.org/10.1002/2015GL066593

Seager, W.R. (1980). Quaternary fault system in the Tularosa and Hueco basins, southern New Mexico and West Texas. *New Mexico Geological Society Guidebook*. 31st conference, Trans-Pecos Region.

Shen, W., & Ritzwoller, M. H. (2016). Crustal and uppermost mantle structure beneath the United States. *Journal of Geophysical Research: Solid Earth*, *121*, 4306–4342. https://doi.org/10.1002/2016JB012887

Shen, W., Ritzwoller, M. H., & Schulte-Pelkum, V. (2013). A 3-D model of the crust and uppermost mantle beneath the central and Western US by joint inversion of receiver functions and surface wave dispersion. *Journal of Geophysical Research: Solid Earth*, *118*, 262–276. https://doi.org/10.1029/2012JB009602

Siripunvaraporn, W., Egbert, G., & Uyeshima, M. (2005). Interpretation of two-dimensional magnetotelluric profile data with three-dimensional inversion: Synthetic examples. *Geophysical Journal International*, *160*(3), 804–814. https://doi.org/10.1111/j.1365-246X.2005.02527.x

Steck, L. K., Thurber, C. H., Fehler, M. C., Lutter, W. J., Roberts, P. M., Baldridge, W. S., et al. (1998). Crust and upper mantle *P* wave velocity structure beneath Valles caldera, New Mexico: Results from the Jemez teleseismic tomography experiment. *Journal of Geophysical Research*, *103*(B10), 24,301–24,320. https://doi.org/10.1029/98JB00750

Tweto, O. (1979). The Rio Grande rift system in Colorado. In R. E. Riecker (Ed.), *Rio Grande rift: Tectonics and magmatism* (pp. 33–56). Washington, DC: American Geophysical Union. https://doi.org/10.1029/SP014p0033

van Wijk, J. W., Baldridge, W. S., van Hunen, J., Goes, S., Aster, R., Coblentz, D. D., et al. (2010). Small-scale convection at the edge of the Colorado plateau: Implications for topography, magmatism, and evolution of Proterozoic lithosphere. *Geology*, *38*(7), 611–614. https://doi.org/10.1130/G31031.1

Walker, J. D., Bowers, T. D., Black, R. A., Glazner, A. F., Farmer, G. L., & Carlson, R. W. (2006). A geochemical database for western north American volcanic and intrusive rocks (NAVDAT). In A. K. Sinha (Ed.), *Geoinformatics: Data to knowledge: Geological Society of America Special Paper 397* (pp. 61–71). Boulder, CO: Geological Society of America. https://doi.org/10.1130/2006.2397(05)

Wannamaker, P. E., Evans, R. L., Bedrosian, P. A., Unsworth, M. J., Maris, V., & McGary, R. S. (2014). Segmentation of plate coupling, fate of subduction fluids, and modes of arc magmatism in Cascadia, inferred from magnetotelluric resistivity. *Geochemistry, Geophysics, Geosystems*, *15*, 4230–4253. https://doi.org/10.1002/2014GC005509

Wannamaker, P. E., Hasterok, D. P., Johnston, J. M., Stodt, J. A., Hall, D. B., Sodergren, T. L., et al. (2008). Lithospheric dismemberment and magmatic processes of the Great Basin-Colorado plateau transition, Utah, implied from magnetotellurics. *Geochemistry, Geophysics, Geosystems*, *9*, Q05019. https://doi.org/10.1029/2007GC001886

Wannamaker, P. E., Hohmann, G. W., & Ward, S. H. (1984). Magnetotelluric responses of three-dimensional bodies in layered earths. *Geophysics*, *49*(9), 1517–1533. https://doi.org/10.1190/1.1441777

Wessel, P., & Smith, W. H. F. (1991). Free software helps map and display data. *EOS, Transactions American Geophysical Union*, *72*(41), 441–446. https://doi.org/10.1029/90EO00319

Wilson, D., Aster, R. C., Ni, J., Grand, S. P., West, M., Gao, W., et al. (2005). Imaging the seismic structure of the crust and upper mantle beneath the Great Plains, Rio Grande rift, and Colorado plateau using receiver functions. *Journal of Geophysical Research*, *110*, B05306. https://doi.org/10.1029/2004JB003492